MET O 19 BRANCH MEMORANDUM No.....48.....

For Revised Assessment see No. 50.

An assessment of the effect of atmospheric liquid water on the retrieval accuracy of an active microwave pressure sounder.

by

T. N. Palmer.

March 1979.

Met O 19
(High Atmosphere Branch)
Meteorological Office
London Road
BRACKNELL
Berks RG12 2SZ

Contents

AM

1 Introduction

In a recent report [1], Flower and Peckham (hereafter FP) discuss the ability of a satellite-borne active multichannel microwave sounder to measure atmospheric attenuation in the microwave O_2 absorption band, and thereby deduce surface pressure over oceanic regions. The purpose of this report is to assess the effect of atmospheric liquid water on retrieval accuracy of the pressure sounder, and outline possible modifications to the FP system in view of the problems posed by liquid water.

FP recommend a 6-channel instrument, 4 channels lying on, or in the vicinity of the 60 GHz O_2 band; one channel lying in the wings of the 22 GHz water vapour line, and one lying in the window region around 35 GHz. Although the instrument principally measures attenuation by O_2, the latter channels attempt to correct for the effects of absorption by H_2O. The instrument is designed by FP to measure the ratio of return power P_{Ri} ($i = 1, \text{---} 6$) between pairs of channels, which are then combined according to

$$S \equiv \prod_{i=1}^{6} \left(P_{R_i} \right)^{r_i} \qquad 1.1)$$

(so $r_1 = -r_2$, $r_3 = -r_4$, $r_5 = -r_6$), and the remaining three free parameters (r_1, r_3, r_5) are chosen such that if a background (ie non-oxygen) atmospheric constituent has an absorption coefficient whose frequency dependence is modellable by a second order polynomial, then S is independent of the amount of this background constituent. In particular FP assume that atmospheric liquid water absorption has this quadratic form. The quantity S, known as the pressure index, is, by simulated retrieval, found to have a linear variation with surface pressure. FP estimate the r.m.s. variance about this best straight line (caused by variability of atmospheric temperature and water vapour distribution) to be 0.4 mb. This variance is a source of retrieval error.

A second source of retrieval error arises from the incoherence of return signals between any two channels. This is the result of backscatter from the specularly reflecting sea surface, and has been demonstrated experimentally by Weissman and Johnson [2]. However, by averaging over a large number of statistically independent return signals, sea-surface backscatter is determined from the mean backscatter cross-section which has known frequency dependence. This averaging may be achieved either by increasing the effective radar footprint in the along-track direction, the numbers of independent samples being obtained from the spatial incoherence length, or by frequency sweeping. For the former system, an effective along-track footprint dimension of 80 km gives a retrieval error of 1.1 mb. The latter system has the advantage of better ground resolution, but as FP discuss, suffers from reduction in signal to noise by at least 8 db over the fixed frequency scheme, and also requires more complex hardware.

Retrieval errors due to atmospheric variability and sea surface backscatter, will always be present and can be combined statistically giving a 'background' error of 1.2 mb.

Further to these, there will be errors in surface pressure retrieval due to attenuation by cloud. This is partially because of loss of signal to noise ratio from liquid water attenuation; but also the variability of cloud liquid thickness significantly reduces the pressure index's insensitivity to liquid water, and is itself a source of inaccuracy. Precipitation increases these errors.

In order to discuss the impact of atmospheric liquid water, it is desirable to have an upper bound on useful retrieval accuracy. Clearly this is a function of the density of conventional meteorological data. In the Northern hemisphere this density is high (except perhaps in the Arctic regions) and 2 mb may well be an upper bound on the usefulness of the system. The Southern hemisphere density is considerably lower, and estimating an upper bound of 3 or 4 mb is perhaps reasonable. It is not claimed that these limits on useful accuracy are other than arbitrary values at this stage. A more detailed study of the requirement, including such factors as the spacial coherence of the errors and spacial coverage of observations, will be made elsewhere. The plan of this report is as follows.

In section 2, retrieval errors will be evaluated for different cloud conditions and in section 3 some measurements of cloud liquid density will be given to assess the significance of the calculations of section 2. Possible modifications to the FP system in the light of the previous sections will be discussed in section 4, and an assessment of global coverage will be made in section 5. Some concluding remarks are made in section 6. A short appendix describes a stochastic model for cloud inhomogeneity.

2 Retrieval accuracy in cloudy conditions

2.1 Uniform cloud

Using the definition of pressure index given by 1.1), the fractional error in S due to a signal to noise ratio N_i in the i^{th} channel, is given by

$$\left(\frac{\delta S}{S}\right)^2 = \sum_{i=1}^{6} \left(\frac{r_i}{N_i}\right)^2 \qquad 2.1)$$

Given output power, receiver noise figures, and other design characteristics (see table 1) then the left hand side of 2.1) may be calculated for various atmospheric and sea surface conditions. Knowing the sensitivity of S to changes in surface pressure, which FP give as

$$\frac{\delta p_s}{p_s} = .13 \times \frac{\delta S}{S} \qquad 2.2)$$

then an estimate of retrieval error due to reduction in signal to noise may be found. This is statistically combined with the 'background' error 1.2 mb. To model these errors, a winter mid-latitude standard atmosphere is used [3]. Oxygen attenuation is determined by the Rosenkranz model [4], water vapour by Van Vleck's model [5], and liquid water by Staelin's model [6], which assumes a Rayleigh absorption regime.

At 2km above the surface, a uniform layer of cloud is added, and total atmospheric transmission computed using the above theoretical models. From the data of FP on sea surface backscatter cross-section, P_{R_i} is calculated, giving signal to noise and, from 2.2, δp_s, the error in surface pressure. In fig. 1 δp_s is plotted against cloud liquid thickness for moderate and rough sea states, with instrumental inclinations of 0° and 14° to nadir. It is assumed that the cloud is mainly in the liquid phase.

Notice from fig. 1, the residual error of 1.2 mb. As cloud liquid thickness increases, retrieval errors increase. For a nadir direction, the 2mb (northern hemisphere) upper bound is reached at a liquid thickness of $\sim 2\frac{1}{2}$ mm for a moderate sea surface, and $\sim$ 2 mm for a rough sea surface. For an instrumental direction of 14° to nadir, the error limit is reached at $\sim 1\frac{1}{2}$ mm of water. These figures are sensitive to cloud temperature; for example, a summer midlatitude atmosphere requires somewhat higher liquid thicknesses to produce the same retrieval errors.

The effect of light precipitation is demonstrated in fig. 2. Calculations were based on the expressions of Gloersen and Barath [7], which assume a Marshall-Palmer drop size distribution. The curves are retrieval errors for a rainfall rate of 1 mm/hr incorporated into the previous cloud model. Comparing figs. 2 and1, one can approximately interpret fig. 2 as a translation of fig. 1 in the Ox direction by 0.3 mm, suggesting a rainfall rate of 1 mm/hr from 2km to be equivalent to $\sim$ 0.3 mm of cloud liquid thickness.

Consideration of rain introduces another problem. For any significant rainfall rate, the rainfall backscatter cross-section will be comparable with the 'effective' sea-surface backscatter, having taken 2-way cloud attenuation into account. Hence, at the receiver, the sea-surface backscattered signal will be contaminated with a raindrop backscattered signal. Treating the latter as noise, then the resulting signal to noise ratio, in db, is given in terms of cloud transmission τ_{water}, sea-surface backscatter cross-section σ_{sea}, and raindrop backscatter cross-section σ_{rain} by

$$N\,(db) \simeq \tau^2_{water}(db) + \sigma_{sea}(db) - \sigma_{rain}(db)$$

Using data in FP, together with 2.1), retrieval errors for a moderate sea-surface with nadir beam are plotted in fig 3 for various rainfall rates falling through 2km and cloud liquid thickness of 1 mm. The curve suggests that for the sounder to probe any significant quantities of rain, integration over the entire return signal will results in substantial retrieval errors.

2.2 Variable Cloud

In the preceding discussion, it was assumed that cloud (or rain) cover was uniform over the 10 x 80 km^2 footprint. With uniform cloud, the assumption that water absorption is modellable by a quadratic polynomial in frequency is a good one. However, if cloud is nonuniform then the assumption is not valid, and a further error is introduced into the pressure estimate.

In their report, FP discuss the effect of broken cloud when uniformly thick cloud covers a fraction of the field of view. They suggest that the effect of broken cloud is most easily mitigated by dividing integration into shorter periods, calculating the index S for each subdivision, and finally averaging S over the total integration time. The problem, however, is that cloud liquid thickness varies over distances smaller than the (instantaneous) radar footprint. Rather than consider a uniform density for continuous cloud cover, it is more realistic to treat liquid thickness as a random variable with given mean, μ , and standard deviation , σ , whose values depend on prevailing conditions. The mathematical details of this stochastic cloud model are given in the appendix, however we shall focus attention on two models

a) $\sigma = \mu/2$

b) $\sigma = \mu/4$

of inhomogeneous cloud cover. In fig 4 retrieval errors due to inhomogeneity are illustrated for models a) and b). It is clear that the effect of non-uniform cloud as represented by these models degrades retrieval accuracy.

Hence, not only does broken cloud present problems to retrieval, but so also does inhomogeneous cloud. FP claim that a three parameter model for liquid water absorption of the form $(a + b\nu^2 + c\nu^4)$ would adequately account for uniform cloud, and at the same time significantly reduce the effect of broken cloud. This statement, however, was not verified by them. To test it, cloud models a) and b) above were used, and exponents r_i calculated such that the pressure index is insensitive to absorption coefficients of the quartic form above. Results are shown in fig. 5.

The effect of cloud inhomogeneity has now been reduced; retrieval error is 2mb for model a) with $\mu = 1.3$ mm of water.

If model a) is physically reasonable, this is not a wholly satisfactory solution to the problem, and in section 4, possible alternative procedures are examined for reducing the effect of broken or inhomogeneous cloud.

3. Typical values of cloud water content

In this section some measurements of cloud liquid density, are examined, in order to assess the impact of the error curves of the previous section on global coverage of the pressure sounder.

3.1 Layer cloud

Measurements of liquid water density in stratocumulus [8] are illustrated in fig. 6. Mean density is about 0.5 g/m^3 . This is a little larger than mean values reported elsewhere [9], and suggests the aircraft was flying near to the level of maximum liquid density. Nevertheless, if we take a mean of 0.5 g/m^3, then a typical stratocumulus layer of thickness 0.5 km has a total liquid thickness of 0.25 mm. Other layer clouds (e.g. Ac) have smaller liquid thicknesses than this. Precipitation is rare and at most very light from these clouds. Consequently, by reference to Fig. 1, their effect on retrieval accuracy is minimal.

3.2 Frontal cloud

Frontal cloud formation, far from being limited to a particular level or cloud type, can embrace the entire troposphere, and all morphological types from stratus to cumulus and cumulonimbus.

The average distribution of water content in warm front clouds over land is illustrated in fig. 7, using data of Burkovskii [10]. The largest water contents were found in a narrow region extending along the frontal surface; the average value of the water content in this region was 0.32 g/m^3, while the maximum was .59 g/m^3. Below the frontal surface, in the region of stratus fractus, there was a local maximum of water content with an average density of .23 g/m^3. Using the densities of fig 7, the total liquid thickness for these warm front systems was calculated, and is plotted in fig. 8.

The precipitation structure of frontal cloud is rather complex [11], with bands of precipitation, and clusters of cells within the bands. Locally, the rainfall rate may be high (see fig 9) but is mostly less than 4mm/hr, and is generally lighter and less extensive in the warm sector than ahead of the

surface front. The rainfall rates at a cold front may be locally very high indeed (see fig 10). Retrieval errors (but not taking raindrop backscatter into account) for a rainfall rate of 3mm/hr, to a depth of 2km, ahead of the front of fig 7 and 1mm/hr behind it, are plotted in fig 11.

Readings from an aircraft flight through cold front cloud [12] are illustrated in figs. 12 and 13. The first diagram is a flight perpendicular to the front at a height of about 4km, the second at 2km. Observations of rain are also reported. The diagrams show local maxima of $\sim$ .7g/kg ($\sim$.5g/m^3) and generally show values compatible with warm front measurements, though embedded convective elements give high local maxima. Figs 6, 12 and 13 suggest that models a) and b) for continuous cloud variability may be adequately realistic.

3.3 Convective cloud

Liquid densities in convective cloud are certainly greater than in layer and frontal cloud. Table 2 gives some values for well developed cumuliform clouds observed over New Jersey and Florida during the summer. In winter conditions, somewhat smaller values may be appropriate. A typical distribution of liquid water in a cumulus congestus has been given by Mason [9], and is illustrated in fig 14. The total liquid content is about 3mm, above the centre. Clearly such clouds are well localised, and mean liquid water over a radar footprint will be considerably less than 3mm. Nevertheless, cloud variability is an important factor in assessing overall error. Precipitation is also an important factor, since rainfall rates from convective cloud can be very much higher than from frontal cloud.

When convection is particularly strong over the ocean, convective elements (ie cumulonimbus cloud) are organised to form open mesoscale cells, whose diameters (see table 3) are typically $\sim$50 kms. With the effective radar footprint of 10 x 80 km^2, the sounder will not, in general, be able to probe these cloud holes without some reduction in sea surface statistics (ie the loss of a number of independent samples of the sea-surface back-scattered signal, as discussed in section 1). An assessment of the increase in

retrieval error resulting from this will be given in section 4.

3.4 Measurements by satellite-borne passive microwave radiometry

FP discuss the results of Staelin et al [13] who attempt to retrieve cloud liquid thickness from 22 and 35 GHz passive measurements with the Nimbus 6 NEMS radiometer. As FP point out, the large angular beam width of the NEMS instrument gives a ground resolution of about 200 x 300 km^2, and therefore these retrievals often are not representative of individual cloud systems. For example, the retrieved value of mesoscale convection cells with cloud walls of $\sim$3 mm liquid thickness may well be less than 1mm. Furthermore, retrieval is based on statistical regression using the 22GHz and 35 GHz brightness temperatures, and, for example, does not contain predictors for sea surface emissivity, which is a function of surface wind speed, the variation of which can significantly affect retrieval values.

4. Modifications to the FP system

Retrieval error is due principally to reduction of signal/noise by attenuation through heavy precipitating cloud, inadequate parametrization of cloud variability and backscatter from rain drops. To attempt to overcome these problems, modifications to the system proposed by FP are considered in this section.

4.1 Signal/noise

For the hardware system, FP have chosen solid state microwave oscillators, either Gunn effect devices or IMPATT (Impact Avalanche Transit Time) diodes. These devices have available power outputs of a few Watts, with efficiencies of around 10% [14]. For their study, FP consider 2W CW as a reasonable (and commercially available) power output for the pressure sounder system. Clearly, signal/noise can be improved by increasing output power. Although solid state devices may in the near future be capable of 10-20W CW output, travelling wave tubes are presently capable of high power outputs (see fig 15). Travelling wave tubes also, apparently, have proven reliability with many thousands of hours of operation in a space-environment, as output stages for satellite communications transmitters. It is therefore of interest to examine the effect on retrieval error by increasing power output. This is illustrated in figs. 16 and 17 for uniform cloud, over a range of liquid thicknesses, with precipitation rates of 3 and 5 mm/hr through 2km, using a nadir beam. Three curves are shown, corresponding to 2W, 10W, 20W (CW) output. As was discussed in section 2, when rainfall rates exceed a few tenths of a mm/hr, then backscatter from rain can be expected to lead to significant retrieval errors (see fig 3). If one is using the power increase to probe through precipitation, then it will be necessary to operate the sounder in a pulsed mode, with precision gating to isolate the sea-reflected signal. Such gating may, in practice, be difficult to achieve. Since raindrop backscatter occurs within a few kilometres above the ground, the satellite height must be known to this accuracy. However, the height of a satellite above the earth's surface will vary by tens and perhaps hundreds of kilometres around its orbit.

Further, path length is dependent on scan angle, and different gating is therefore necessary for the off-nadir beam to the nadir beam. Some degree of success, however, should be obtainable by operating a pulsed mode, but with implicit gating, ie integrating only over the back end of the return pulse. It is assumed that effects of multiple scattering are unimportant here. Calculations of Uzunoglu and Evans [22] confirm this.

Coverage may also be increased with higher power output by increasing the off-nadir beam angle. With the FP system, 14° beam separation implies 200km measurement separation on the sea-surface. If each measurement has an independent retrieval error of 1.5 mb, then a typical pressure gradient of 3mb/200km perpendicular to the satellite track will be measured with an expected error of 70%. By increasing power output by a factor α, a larger angle, θ, can be attained for the same signal/noise values. θ is determined by the sea-surface backscatter cross section

$$\sigma(\theta) = \sigma(14)/\alpha$$

Using data from FP, with 'moderate' sea conditions, a 10W output allows angles up to about 19° off nadir, and a 20W output allows angles up to 25° off nadir, in which case the 1.5×10^{-2} mbkm^{-1} gradient can be determined with 37% expected error, again assuming measurements with independent errors of 1.5 mb.

A third possible advantage of power increase would be the ability to choose frequencies further into the oxygen band, which would then have the effect of reducing the sensitivity of cloud absorption compared to oxygen absorption, and this might help alleviate the cloud variability problem. Unfortunately O_2 absorption increases so rapidly above 52 GHz, that signal/noise problems become very significant and little inroad into the band could be made without a very substantial increase in power output. Secondly, temperature dependence of O_2 absorption becomes increasingly significant

towards the centre of the band. Hence, it is unlikely that this third suggestion would be of much value.

4.2 Cloud variability

As has been shown, cloud variability presents serious problems for the FP system. Two lines of attack suggest themselves. Firstly, channel frequencies and power exponents could be optimised by explicitly incorporating variable cloud models into an optimisation function. In general such a scheme would not choose exponents in simple pairwise ratios, and a system based on the results of the scheme would differ from the FP system in that absolute attenuation measurements would be necessary. Secondly if cloud is sufficiently well broken, then the sounder may be able to probe through holes in cloud.

An investigation of the first method is being conducted by Gately [15]. He attempts to construct a function such that, when minimised (by a numerical program), it will choose frequencies and exponents for the system that i) maximise pressure dependence, ii) minimise effects of signal statistics and reciever noise, iii) minimise temperature, water vapour, and cloud dependences. His results are, to date, rather disappointing. The minimisation procedure does not produce satisfactory dependences for these three types of variable, the cloud term often being the most troublesome. Also, the dependences are very sensitive to changes in channel frequency, power exponent, and cloud absorption model. It is not clear to what extent these sensitivities are numerical or physical. Gately's research is continuing.

One aspect that may be worth persuing is the construction of a pressure index out of non-linear combinations of absorption coefficients (in 1.1 the exponent of S is linear in absorption coefficients). It is interesting to note that Westwater [16], in attempting to retrieve temperature profiles by passive microwave radiometry, corrects for cloud by a quadratic regression of brightness temperatures. Optimisation of a 'non-linear pressure index' may achieve more satisfactory results.

Alternatively some use could be made of independent measurements from passive sounders for temperature and liquid water retrieval, or indeed the pressure sounder itself could be operated with different power exponents that maximised temperature or liquid water dependence, while minimising pressure dependence; and an iterative correction procedure applied.

It is unlikely that problems of cloud variability will be completely solved. Gately's work suggests that these variability errors will be worst when cloud covers some 90% of the field of view, and leaving 10% clear. In these situations, when cloud is thick, it may be best simply to ignore such measurements. Hence, in the following, we shall either assume that holes are sufficiently large to sound through, or that when sounding through continuous cloud cover, variability errors can be modelled by curve b) in fig 5). A crude estimate of precipitation variability can be made by assuming 2km of rain at a rate of 1mm/hr is equivalent to .3mm of cloud water (see section 2).

The principle error in sounding through holes in cloud is the loss of sea-surface statistics. As stated in section 1, FP deduce for an effective along-track resolution of 80km the statistical error will be 1.1mb. To calculate statistical errors for smaller effective resolutions, we need the instantaneous along-track radar footprint. At 60 GHz this is 9 km (the value is obtained by calculating the first minimum of a diffraction limited aperture, and is clearly wavelength dependent.) Hence, if the spacial coherence length of the reflecting surface is δx(km), and the number of independent samples is N then

$$(9 + N\delta x) = 80$$

So, for an effective resolution of ℓ km, the number of independent samples N' is given by

$$(9 + N'\delta x) = \ell$$

and the statistical retrieval error is

$$e = 1.1\sqrt{\frac{N}{N'}} \quad \text{mb}$$

$$= 1.1\sqrt{\frac{71}{\ell - 9}} \quad \text{mb}$$

A plot of e against ℓ is given in fig 18. It is seen that resolution for the upper bound error of 2mb is 30km. Hence the system will be able to probe through cloud-free holes of 30km or move with satisfactory retrieval accuracy. To implement this, attenuation at each basic radar footprint must be analysed, to isolate the cloud free regions, before being integrated together to give an effective footprint within a hole. Hence, using the data in table 3, useful pressure retrievals are capable of being made in a typical field of open convective cells, when individual clouds are too thick to probe.

Finally, there may be problems both because the 3 db beamwidth is frequency dependent, and the signals are not beamed simultaneously, leading to instrument channels measuring different parts of the atmosphere. This may be important in attempting to correct for cloud cover which can change very abruptly.

5. Assessment of global coverage

In this section, total retrieval errors for four meteorological conditions (no cloud, non-raining cloud, weakly raining cloud and moderate or heavily raining cloud) are assessed. For conciseness, results are presented in table 4.

The global coverage of the FP system is shown in fig. 19, where part of a 25° swath is also illustrated. To assess the effect of precipitation on this coverage, oceanic precipitation rates have been studied, using data from the Electrically Scanning Microwave Radiometer (ESMR) on Nimbus 5 and Nimbus 6, [20] [21]. A limitation of the ESMR is that its threshold sensitivity to precipitation at mid-latitudes is rather high; the threshold is about 4mm/hr through a depth of 4km. Some results are illustrated in figures 20-22. In fig 20, apart from the continuous belt of rain in the tropics, precipitation from a mid-Atlantic mid-latitude frontal system can clearly be seen. The frequency of precipitation ($\geq$ 1mm/hr through 4km) for a given location in the tropics is shown in fig.22. The results broadly indicate that rain will prevent about 10% of soundings in the tropical regions.

To show rainfall frequency in mid and high latitudes, 3 numerical rainfall forecast charts are illustrated in figs. 23-25. Isopleths are in intervals of .2mm/hr. Between the.2 and .6 mm/hr isopleths, soundings may be intermittant, being prevented by local concentrations of rain. Inside the .6 mm/hr isopleth soundings may be very occasional, relying on sounding through 'holes' in the rain belts, (in such a situation, a 'hole' may still be cloudy). Figures 23-25 give only an approximate indication of oceanic rainfall, but from them we may estimate that overall there should be less than 10% loss of coverage due to rain.

6. Conclusions

The FP system is clearly not designed to sound through rain, suffering from signal/noise, cloud variability and raindrop backscatter problems. An attempt has been made to define and quantify the degradation in accuracy associated with these effects. If it were technically feasible (and this is not clear), a pulsed, gated (implicit or explicit) system with power output of 10-20W would significantly reduce signal/noise and raindrop backscatter problems, but not cloud variability. This latter source of error is the subject of continuing investigation. In a recent communication [23], Flower confirms the problems of broken cloud. If 25% of the radar footprint is cloud-free, then by sounding through a cloud of 1mm liquid thickness, up to 7mb retrieval error can be expected from variability factors. In this paper we have assumed that measurements from such situations must be ignored; and we have modelled inhomogeneities in continuous cloud cover stochastically (curve b) fig.5.

With the FP system, it may be preferable to probe through holes in precipitating cloud, and trade off loss in sea-surface coverage against errors due to signal/noise, variability and raindrop backscatter. This will be particularly relevant in retrieving through mesoscale open cell convection which is frequent, and often very extensive in the polar air behind cold fronts.

In Flower's communication, he raises an important point that can only be decided by the user requirement. In assessing the design parameters, in particular the antenna radius, it is of importance to know whether to minimise the overall error in global pressure measurements, or degrade the performance so that measurements can be extended to perhaps an additional 1-3% of situations. In other words, is maximising coverage more important than minimising retrieval error; if not, what is the optimum trade-off? Flower's estimate of coverage is shown in fig.26, and broadly agrees with the conclusions of this report. Clearly, however, a reliable estimate of the distribution of errors requires a good data

base of oceanic cloudiness, rainfall distribution and sea-surface wind-speeds. The overall indications are, however, that measurements can be made to within 2mb for about 85% of oceanic soundings.

References

1. Flower D.A. and G.E. Peckham. (1978). A Microwave Pressure Sounder. JPL Publication 78-68 and NASA contract report CR-157567.
2. Weissman D.E. and J.W. Johnson. (1977). IEEE Trans. AP-25, 74.
3. McClatchey R.A. et al (1972). Optical Properties of the Atmosphere. AFCRL Enirn. Res. Pap. No. 411.
4. Rosenkranz P.W. (1975). IEEE Trans. Antennas Propag. AP-23, 498.
5. Van Vleck J.H. (1947), Phys. Rev. 71, 425.
6. Staelin D.M. (1966), J. Geophys. Res. 71, 2875.
7. Gloersen P. and F.T. Barath. (1977). IEEE J. Oceanic Engineering. OE-2. 132.
8. Met O 15 Internal Report.
9. Mason B.J. (1957). The Physics of Clouds, OUP.
10. Burkovskii S.N. (1959). Trudy Ts AO No.28.
11. Harrold T.W. and Austin P.M. (1974). Journal de Recherches Atmospheriques. 8, 41.
12. Met O 15. Internal Report.
13. Staelin, D.M. et al (1976) J.A.M 15, 1204.
14. (1973). Handbook of Remote Sensing Techniques. A survey prepared by EMI Electronics Ltd for the Department of Trade and Industry under contract K46A/59.
15. Gately C. (1978). Internal Report. Dept. of Physics. Heriot-Watt University.
16. Westwater E.R. (1976). Feasibility of Atmospheric Temperature Sensing from Ocean Data Buoys by Microwave Radiometry. NOAA Technical Report ERL 375-WPL 48.
17. Borovikov A.M. et al. (1963). Cloud Physics. Israel Program for Scientific Trnaslations. Jerusalem.
18. Valley S.L. (Ed) (1965). Handbook of Geophysics and Space Environments, McGraw-Hill.
19. Palmer T.N. (1978). Cellular Convection in the Atmosphere. Met.Office. College. Internal Report.
20. Wilheit T.T. (1975). The Electrically Scanning Microwave Radiometer (ESMR) Experiment, in the Nimbus 6 User's Guide. NASA/Goddard Space Flight Center, Greenbelt, MD.

21. Kidder S.Q. (1976). Tropical Oceanic Precipitation Frequency from Nimbus 5 Microwave Data. Dept. of Atmospheric Science. Colorado State University. Collins. Atmos. Sc. Paper No. 248.

22. Uzunoglu N.K. and B.G. Evans. (1978). J. Phys.A 11, 767.

23. Flower D.A. (1979). private communication.

Appendix

A stochastic model for continuous cloud.

Measurements of liquid water density through clouds reveal rapidly fluctuating values in the horizontal, and due to up- and down-currents these values are likely to be correlated in the vertical. Hence it is reasonable to model liquid thickness for continuous cloud cover by a random variable, x, whose probability distribution function

$$g(x) = \beta(m)\, x^m e^{-ax^2} \qquad (0 \leq x < \infty)$$

has two ajustable parameters, a and (integer) m. The normalising factor, $\beta(m)$, is given by

$$\beta(m) = \frac{2a^{\frac{m+1}{2}}}{\Gamma\left(\frac{m+1}{2}\right)}$$

where Γ is the gamma function. The mean, μ, and variance, σ^2, of x are given by

$$\mu = a^{-\frac{1}{2}} \frac{\Gamma\left(\frac{m+2}{2}\right)}{\Gamma\left(\frac{m+1}{2}\right)}$$

and

$$\sigma^2 = \mu^2 \left[\frac{\Gamma\left(\frac{m+1}{2}\right)\Gamma\left(\frac{m+3}{2}\right)}{\Gamma^2\left(\frac{m+2}{2}\right)} - 1 \right]$$

Assume the result of averaging the transmission due to cloud over the radar footprint is equivalent to finding

$$\langle \tau^2_{(cloud)} \rangle = \int_0^\infty \tau^2_{(cloud)}(x)\, g(x)\, dx$$

and that

$$\langle S_c \rangle = \prod_i \langle \tau^2_{(cloud)\,i} \rangle^{r_i}$$

is the corresponding index for cloud. For uniform cloud $S_c = 1$. The retrieval error for inhomogeneous cloud is, therefore, proportional to $|1 - \langle S_c \rangle|$

For m = 1 and m = 9, the following relationships hold between σ and ν, giving rise to cloud models a) and b) in the text

$$\sigma = .52\,\nu \quad \text{if } m = 1$$

$$\sigma = .25\,\nu \quad \text{if } m = 9.$$

ν_i	Operating Frequencies (GHz)	29.2555 36.5555	44.80 52.80	67.51 73.01
r_i	Power exponents	-1 1	1.6 -1.6	-1 1
	Receiver noise equivalent power ($W \times 10^{-17}$)	2.2 2.2	2.4 2.6	2.7 2.7
P_T	Transmitter power	2W		
η_T, η_R	Feed efficiencies	0.85		
(r)	Antenna dimensions	20 x 150 cm		
t	Integration time	12 s		
D	Duty cycle	0.166		
h	Satellite altitude	500	800	km
V	Satellite speed	7.61	7.45	kms^{-1}
Δf	Receiver bandwidth	76.1	74.5	kHz
2h/c	Pulse length	3.33	5.33	ms

Table 1

Design characteristics of the microwave sounder.

Adapted from Table 10 of ref. 1 by addition of information included in text of ref .1

Clouds		Water Content ($g\ m^{-3}$)	
Type	Temp (^oC)	Average	Maximum
Cumulus Humilis	10 to 24	1.0	3.0
Cumulus Congestus	3 to 11	2.0*	6.6
Cumulonimbus	10 to -8	2.5	10.0

* estimated

Table 2 Observed Liquid Water Content of Cumulus Type Clouds Over New Jersey and Florida During the Summer

From [18]

CASE NUMBER	DATE	STATION	STATION CIRCLE	HEIGHT OF CELL (km)	DIAMETER OF CELL (km)
1	25/1/78	OWS R	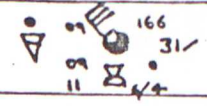	5.7	81
2	24/1/78	OWS L	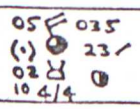	4.9	50
3	19/1/78	OWS R	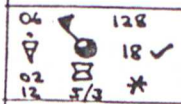	4.8	53
4	16/1/78	Valentia	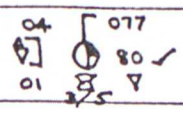	4.6	89
5	16/1/78	OWS R	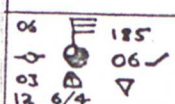	3.4	32
6	14/11/77	OWS L	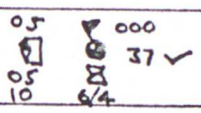	3.3	45
7	14/11/77	Stornoway	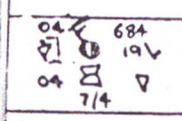	6.3	48
8	7/11/77	OWS L	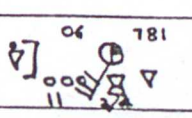	6.1	70
9	3/11/77	OWS L	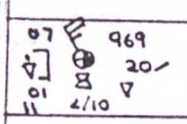	5.8	46
10	31/10/77	OWS L	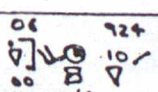	4.0	39
11	31/10/77	OWS R	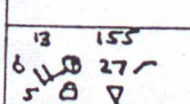	3.7	52
12	27/10/77	Valentia	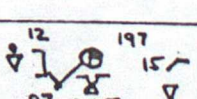	2.6	34
13	12/5/77	OWS L	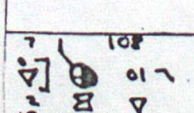	3.7	82

Table 3

Height and diameter of 13 typical midlatitude mesoscale open cells, together with local station circles. From [19]

Table 4. Summary of expected retrieval accuracy for the FP system, assuming moderate sea-surface roughness.

Meteorological conditions	Retrieval accuracy (mb)		Remarks
	nadir	14^{o}	
no cloud	1.2	1.2	Error due to sea-scatter statistics and atmospheric variability. Significant drop in signal/noise at 14^{o} if sea is calm.
continuous but inhomogeneous non-precipitating cloud (liquid thickness=1mm)	1.2	1.6	footprints containing small regions of clear sky must be ignored.
weakly-precipitating continuous cloud (liquid thickness = 1.3mm, rainfall rate = 1mm/hr through 2km)			see fig 5
a) ignoring raindrop back-scatter	1.5	3.5	requires some form of gating and pulsing to isolate sea-surface back-scattered signal
b) with raindrop back-scatter	7	9	
Moderate or heavy precipitation	Very large errors		
Clear holes in mesoscale cellular convection conditions where clouds are raining	2	2	for 30km along-track clear hole.
	3	3	for 20km along-track clear hole.

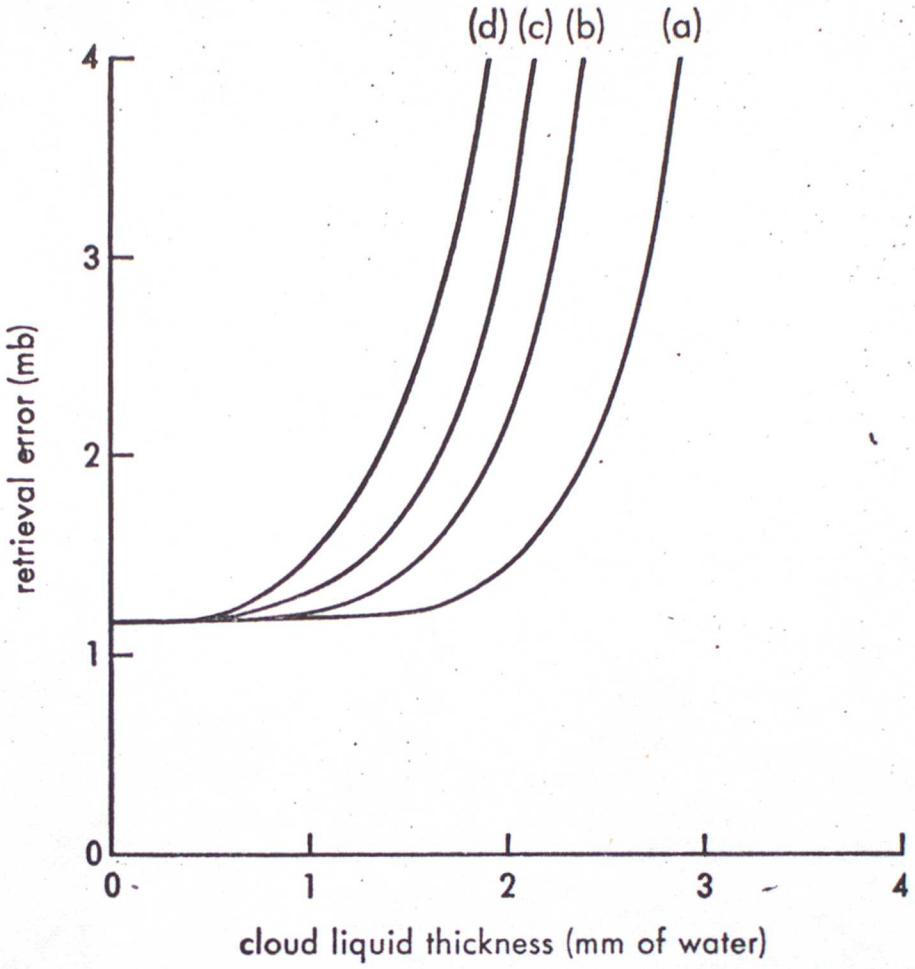

Figure 1.

Retrieval errors for uniform cloud. Winter mid-latitude standard atmosphere.

(a) Nadir beam, moderate sea.
(b) Nadir beam, rough sea.
(c) 14° beam, rough sea.
(d) 14° beam, moderate sea.

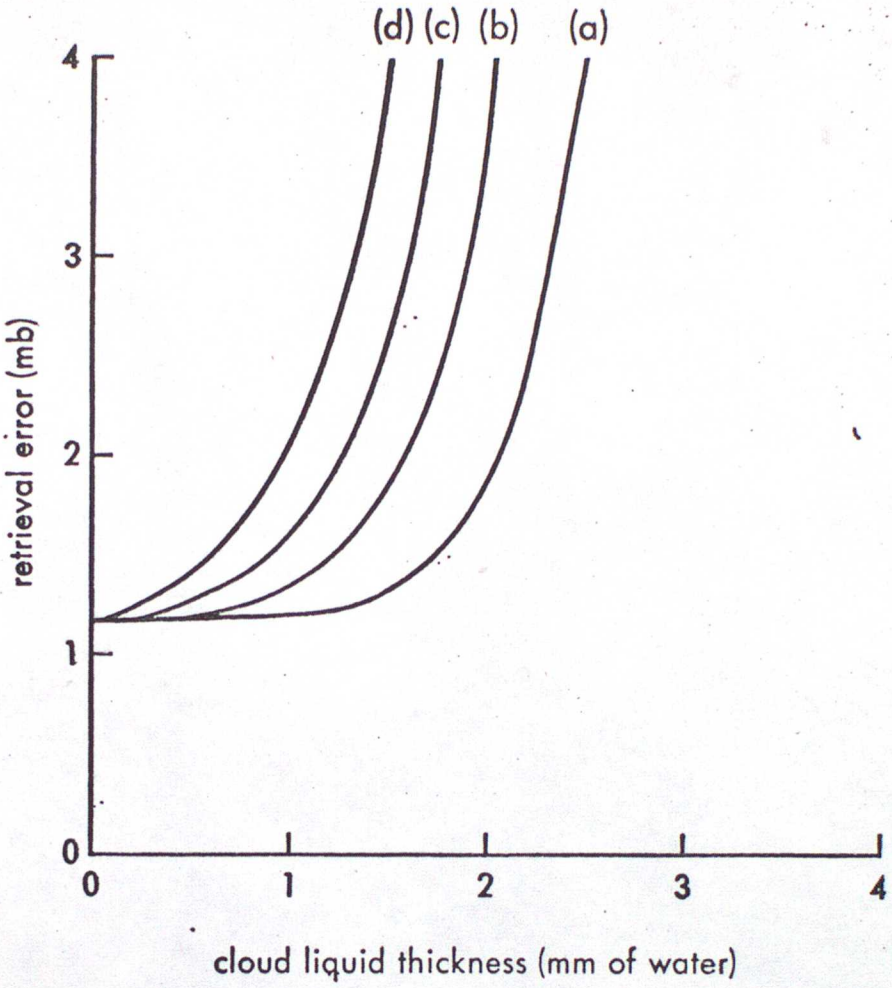

Figure 2.

Retrieval errors for uniform cloud with 1 mm/hr uniform rainfall rate through 2 km depth. Winter mid-latitude standard atmosphere.

(a) Nadir beam, moderate sea
(b) Nadir beam, rough sea
(c) 14° beam, rough sea
(d) 14° beam, moderate sea

Raindrop backscatter error not included.

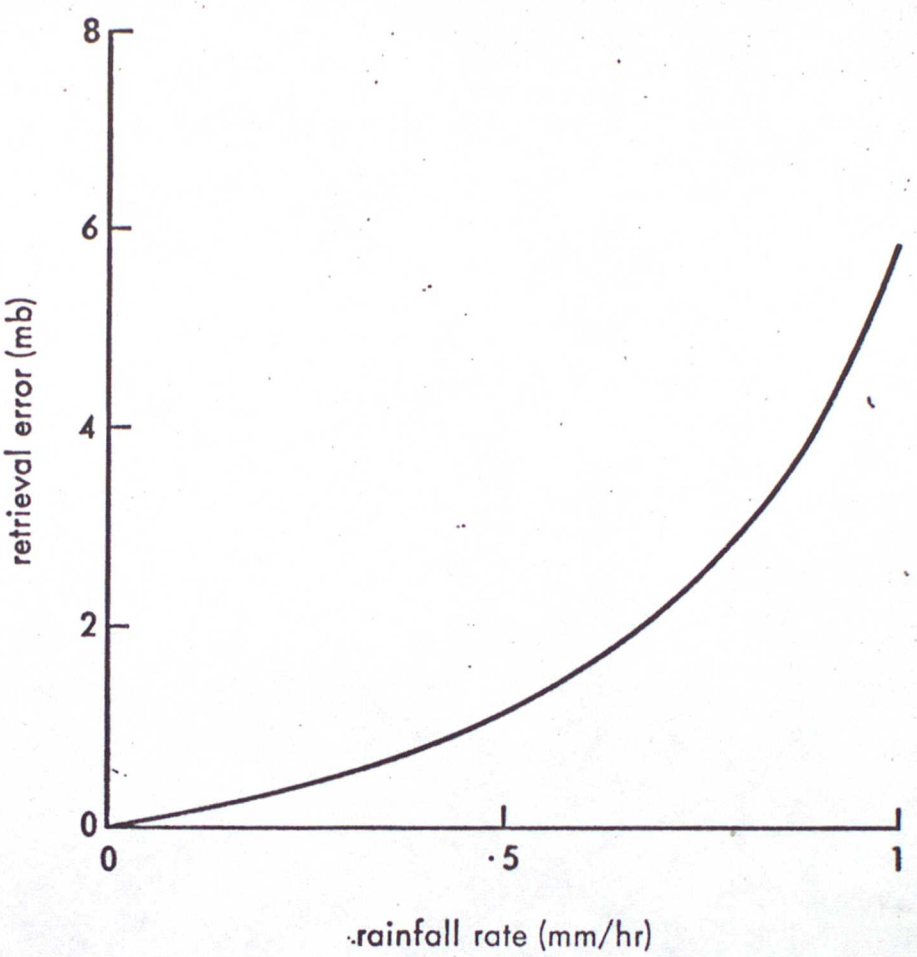

Figure 3.

Retrieval error due to contamination of sea-surface backscattered signal by raindrop backscattered signal (treated as noise). Rainfall is assumed to be falling through 2 km.

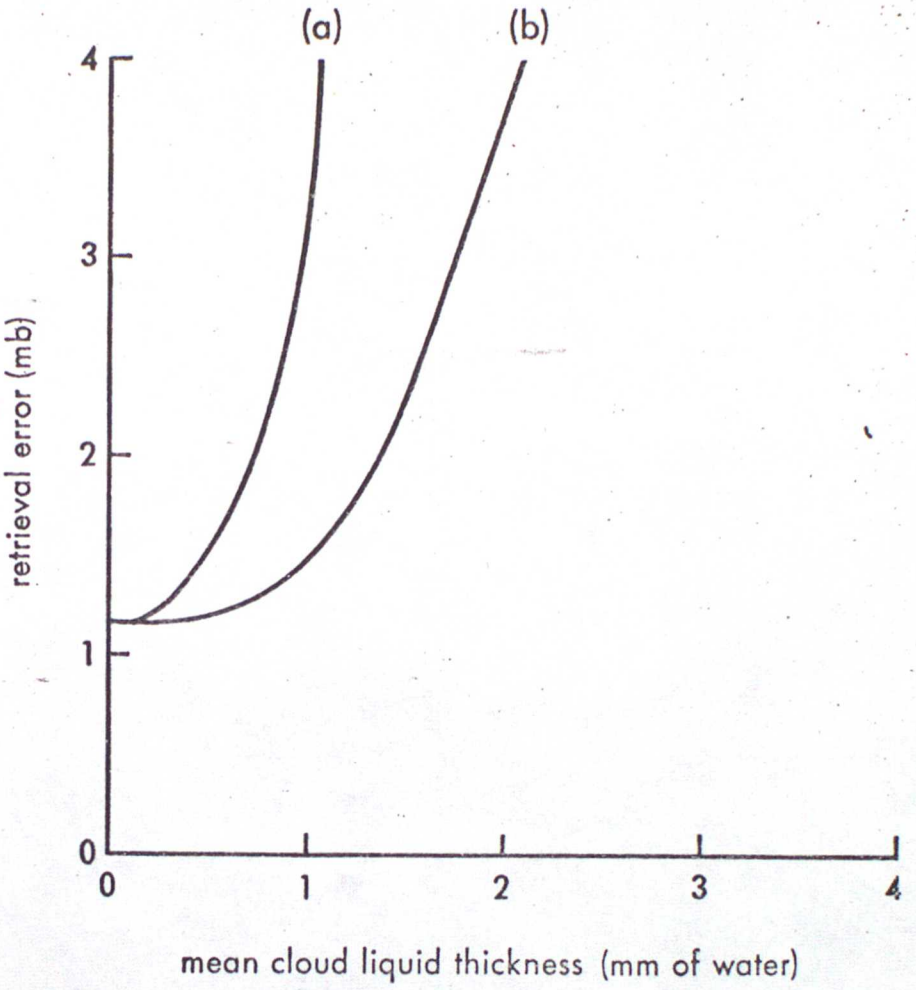

Figure 4.

Retrieval errors for inhomogenous cloud, assuming cloud absorption is modellable by a quadratic polynomial in frequency.

(a) $\sigma = \mu/2$

(b) $\sigma = \mu/4$

(see text)

Moderate sea state, nadir beam. Winter mid-latitude standard atmosphere.

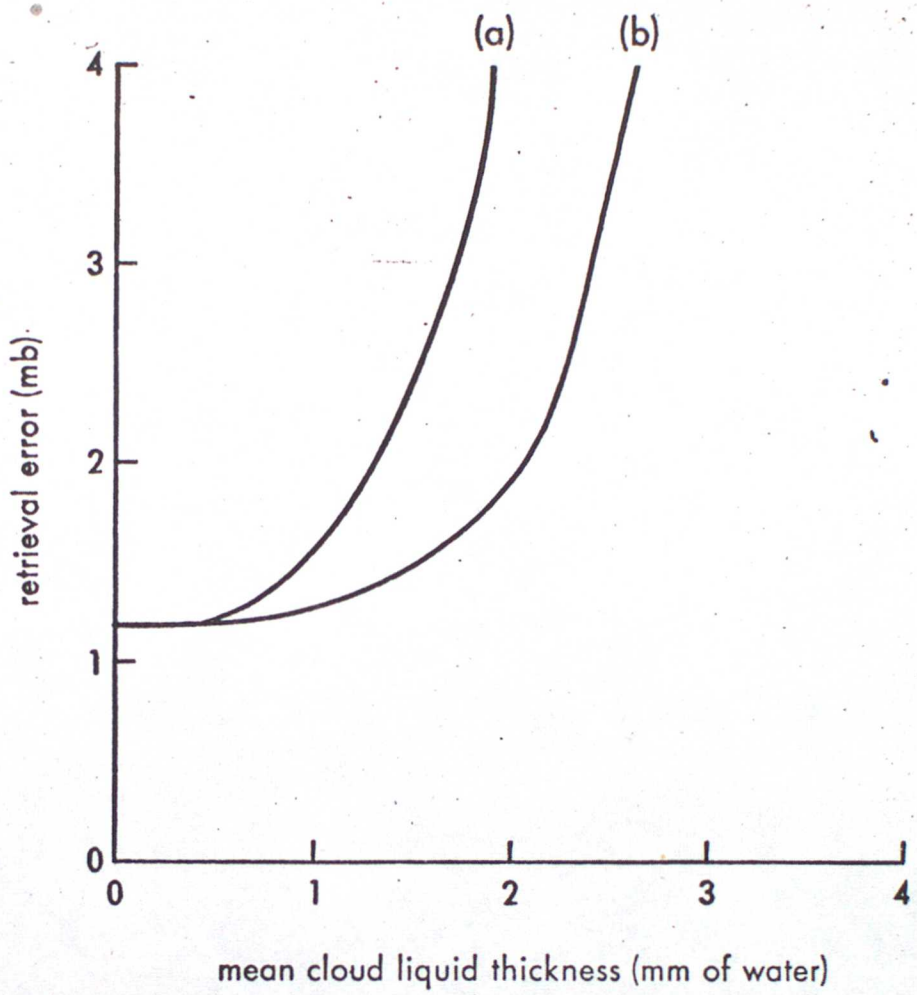

Figure 5.

Retrieval errors for inhomogenous cloud, assuming cloud absorption is modellable by a quadratic polynomial in (frequency)^2.

(a) $\sigma = \mu/2$

(b) $\sigma = \mu/4$

(see text)

Moderate sea state, nadir beam. Winter mid-latitude standard atmosphere.

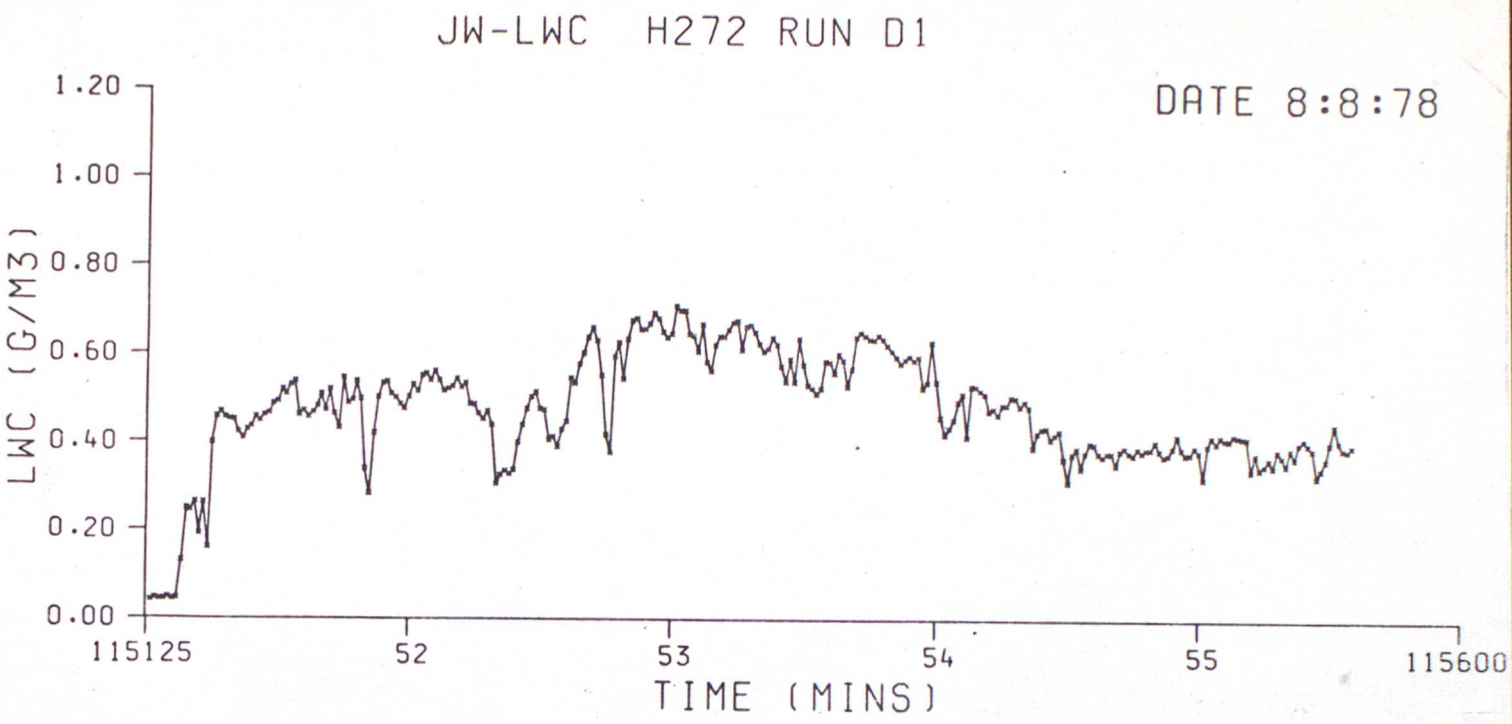

Figure 6

Measurements of liquid water density in stratocumulus

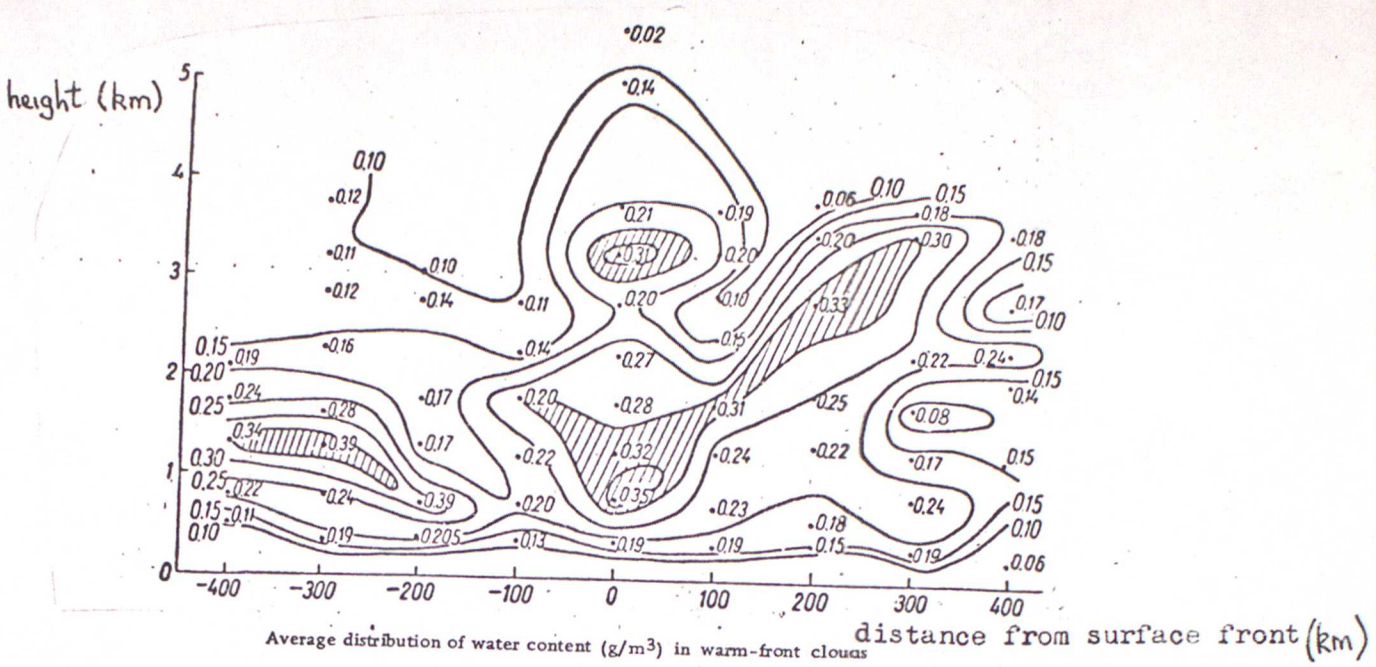

Average distribution of water content (g/m³) in warm-front clouds

Figure 7

From [10]. See also [17]

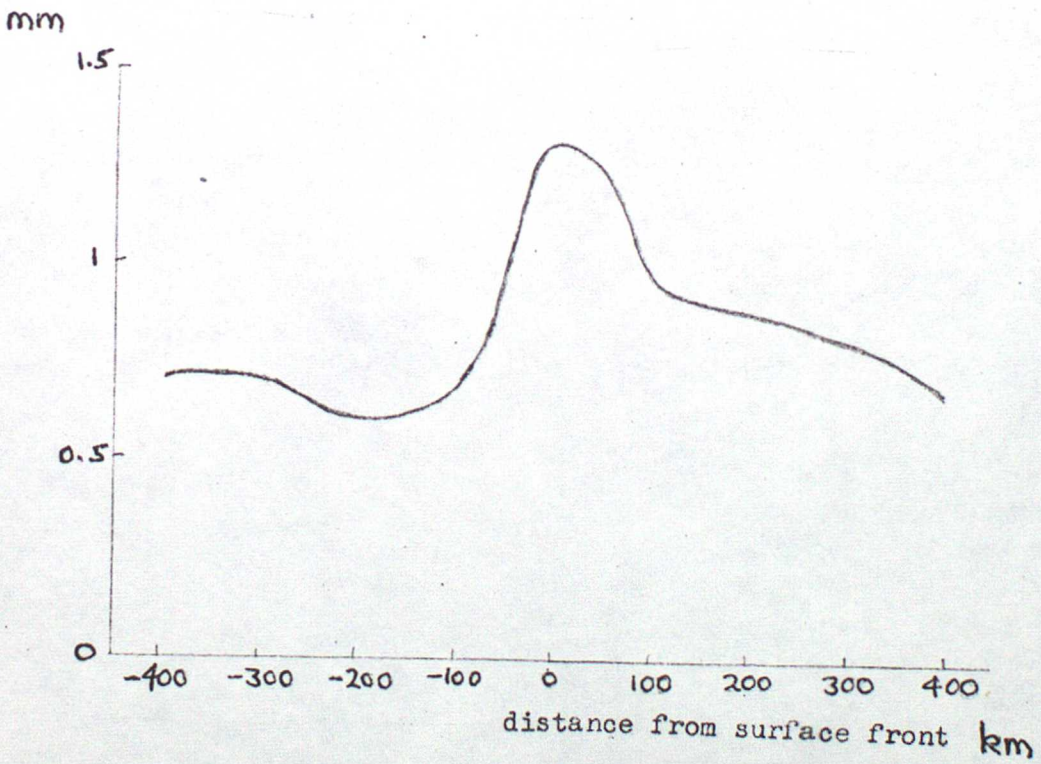

Figure 8

Total water content (mm) derived from figure 7

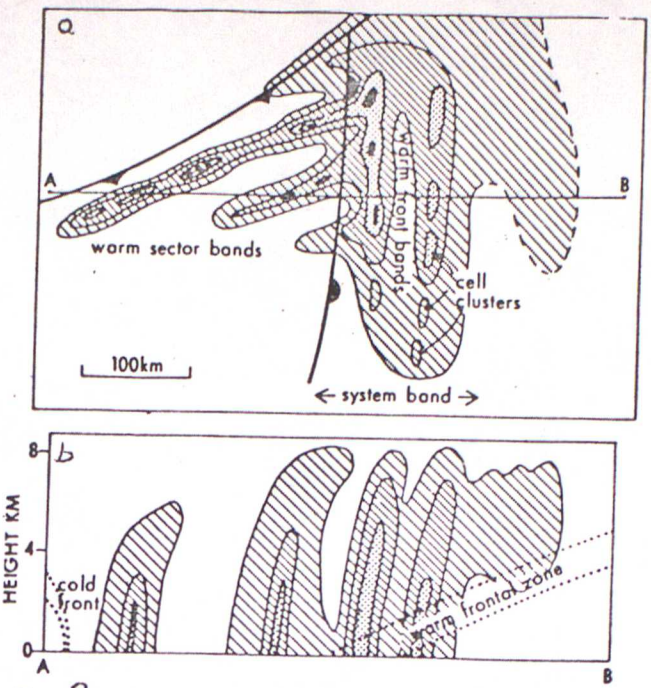

FIG. 9 — Structure of rate of precipitation within a partially occluded cyclone. Isopleths denote precipitation rates of 0.5 mm h^{-1} (outer line), 4 mm h^{-1}, 8 mm h^{-1} and more than 16 mm h^{-1} (solid shading). The dashed portion on the forward side of the system evaporates before reaching the ground.

FIG. 9. — Height-distance section along AB in Fig.

From [11]

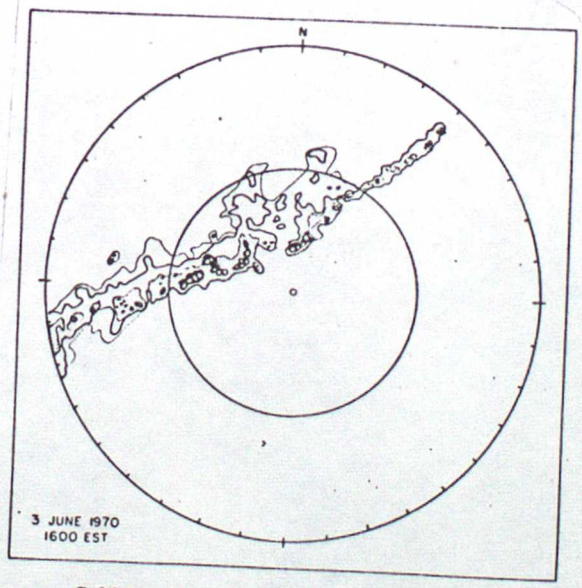

Cold-frontal band observed with 10-cm radar at Cambridge, Mass.
Range : 200 km.
Contours : 1, 3, 10, 35 (black) and > 70 (white spots) mm hr^{-1}.

Figure 10

From [11]

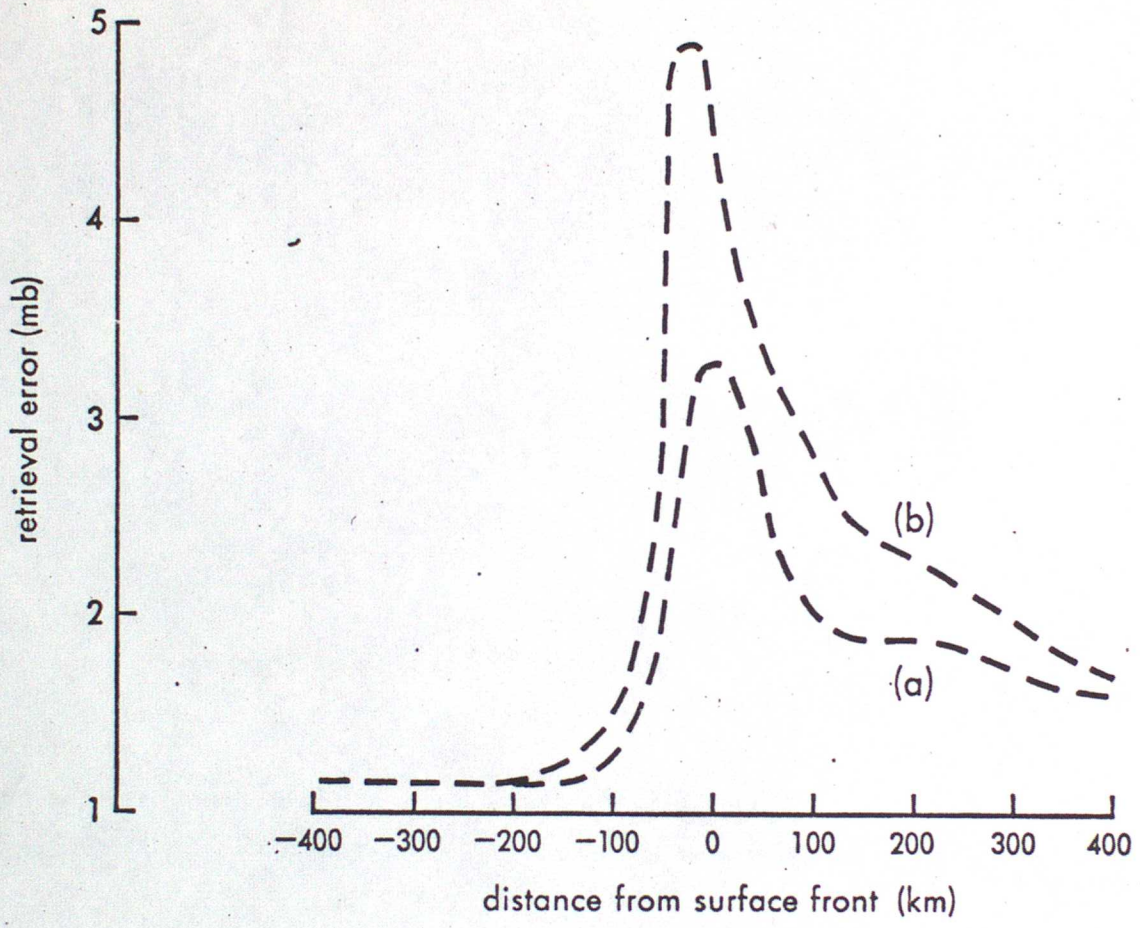

Figure 11.

Retrieval error (ignoring raindrop backscatter) of warm front system of Fig. 7.

(a) Ignoring cloud and rain variability.

(b) Modelling variability by curve (b) in Fig. 5.

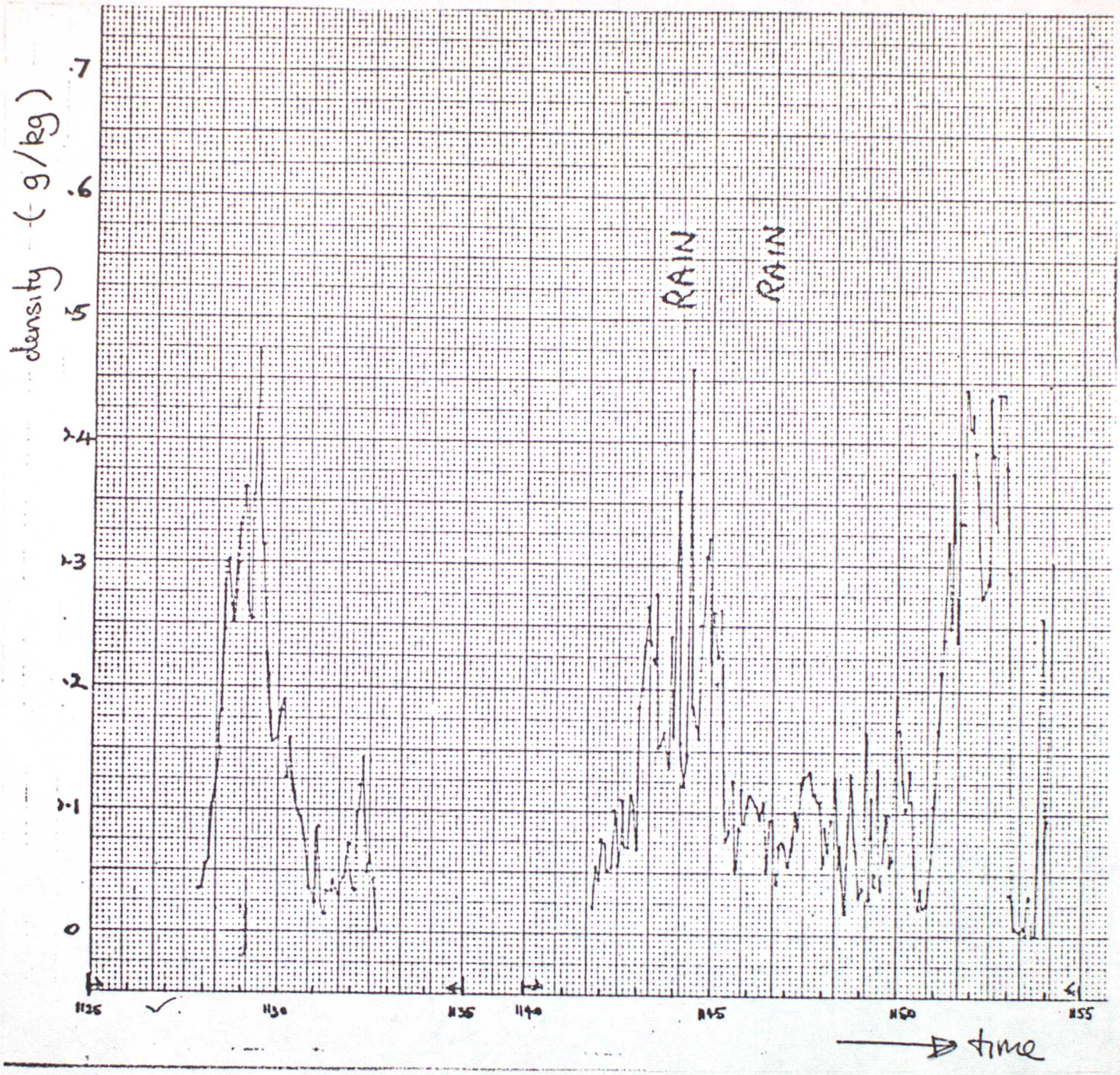

Figure 12

Measurements at 4km of liquid density (g/kg) through a cold front

Figure 13

Measurements at 2km of liquid density (g/kg) through a cold front

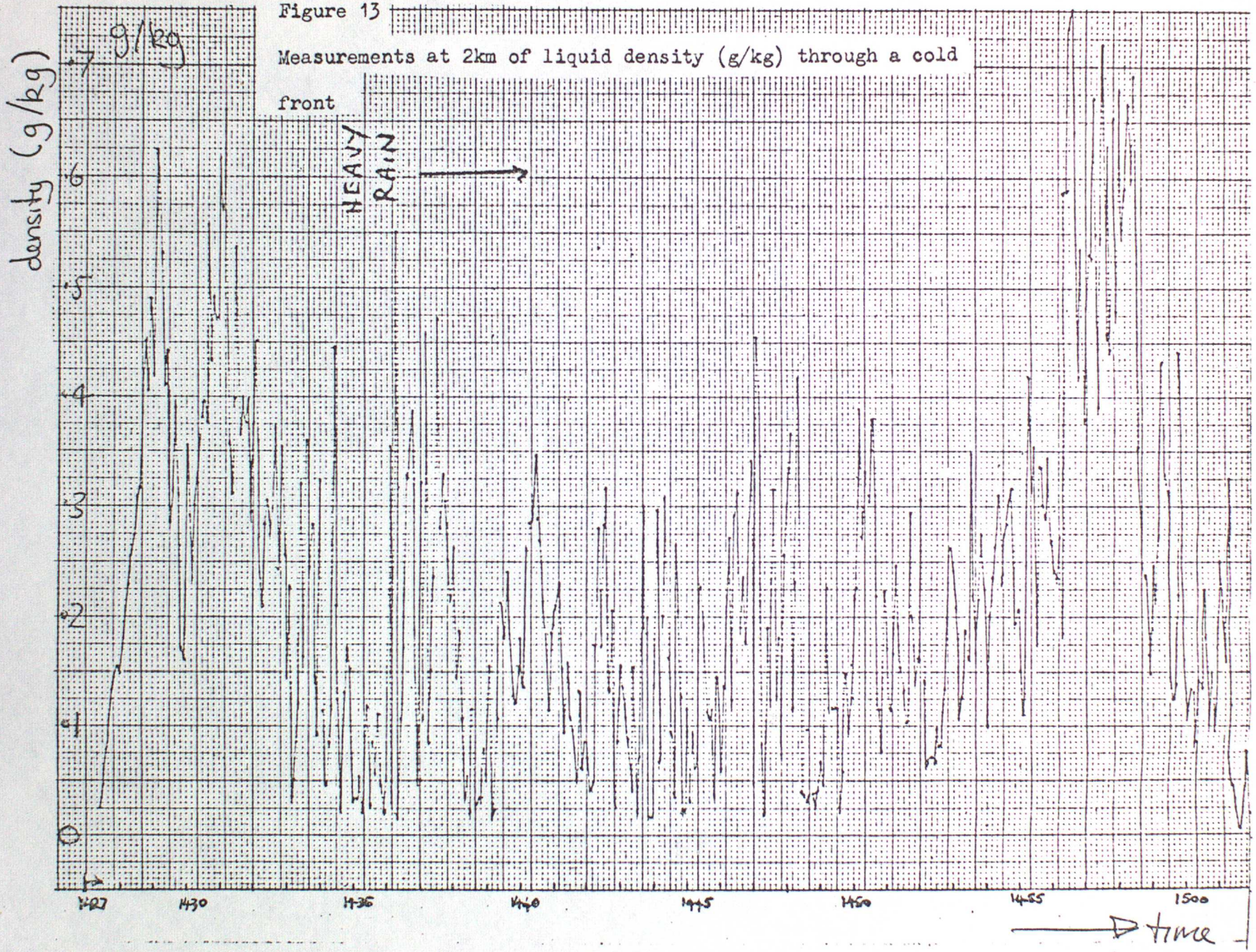

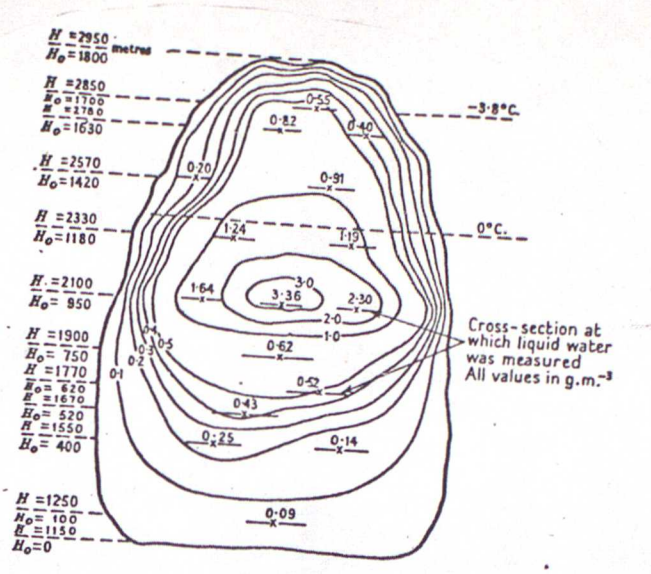

The distribution of liquid water in a cumulus congestus

Figure 14

From [9]

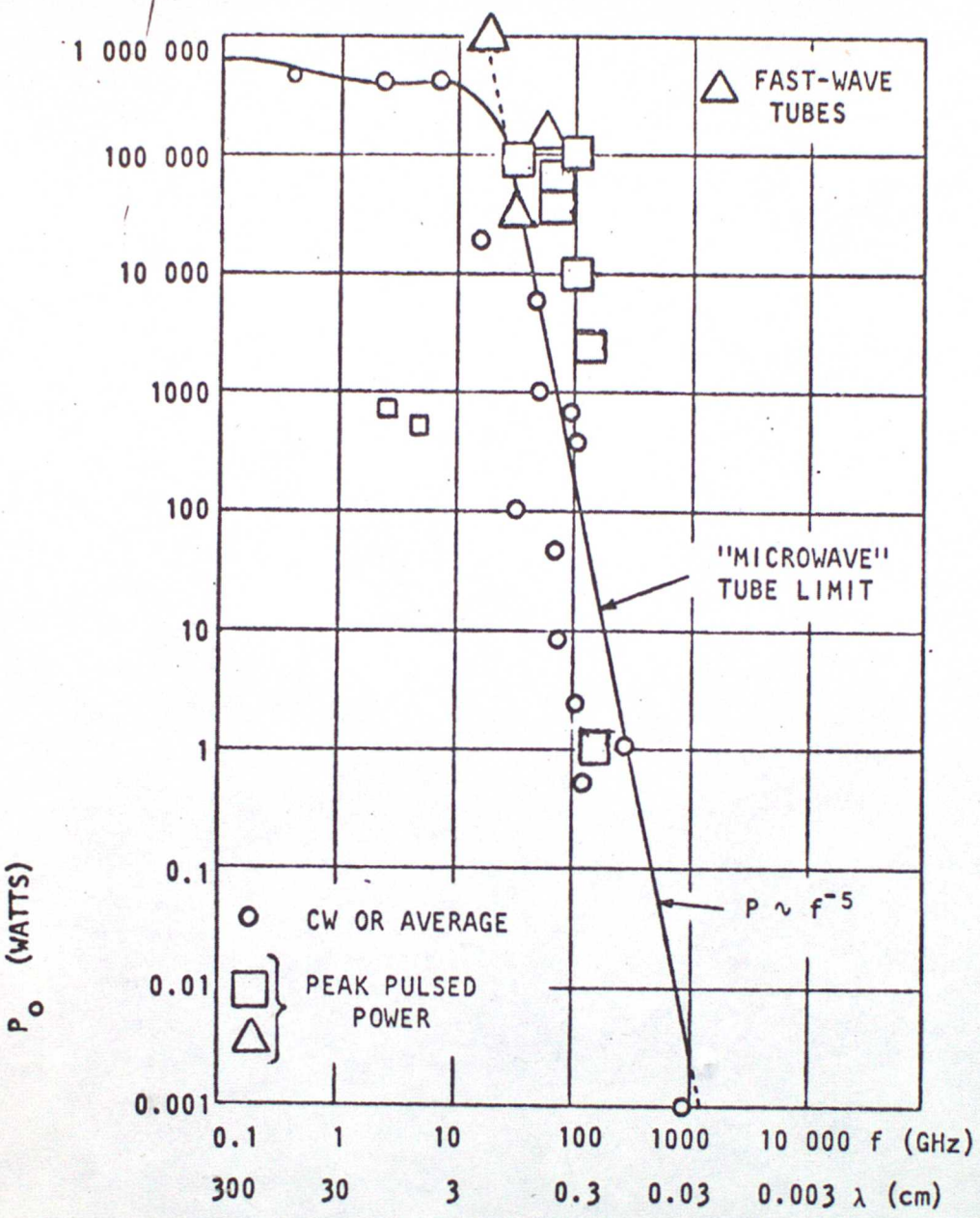

Note 1. Peak Power up to 30 MW available at Lower Microwave Frequencies.

2. Limit plotted for CW or Average Power

3. Data Excludes Information on Classified Tubes.

FIG. 15 FRONTIER MICROWAVE TUBES - 1969 STATE OF THE ART

From [14]

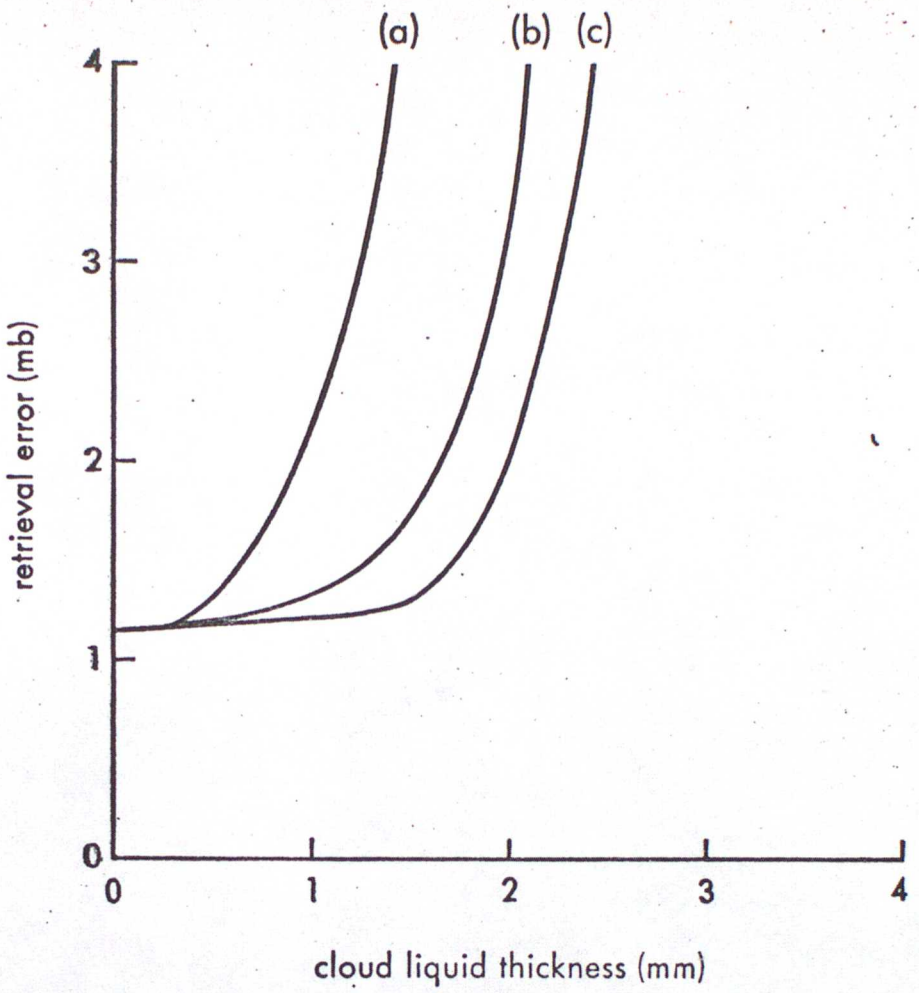

Figure 16.

Retrieval error for uniform cloud with 3 mm/hr uniform rainfall rate. Moderate sea-surface, nadir beam. Winter mid- latitude standard atmosphere.

(a) Output power = 2W CW
(b) Output power = 10W CW
(c) Output power = 20W CW

Raindrop backscatter error not included.

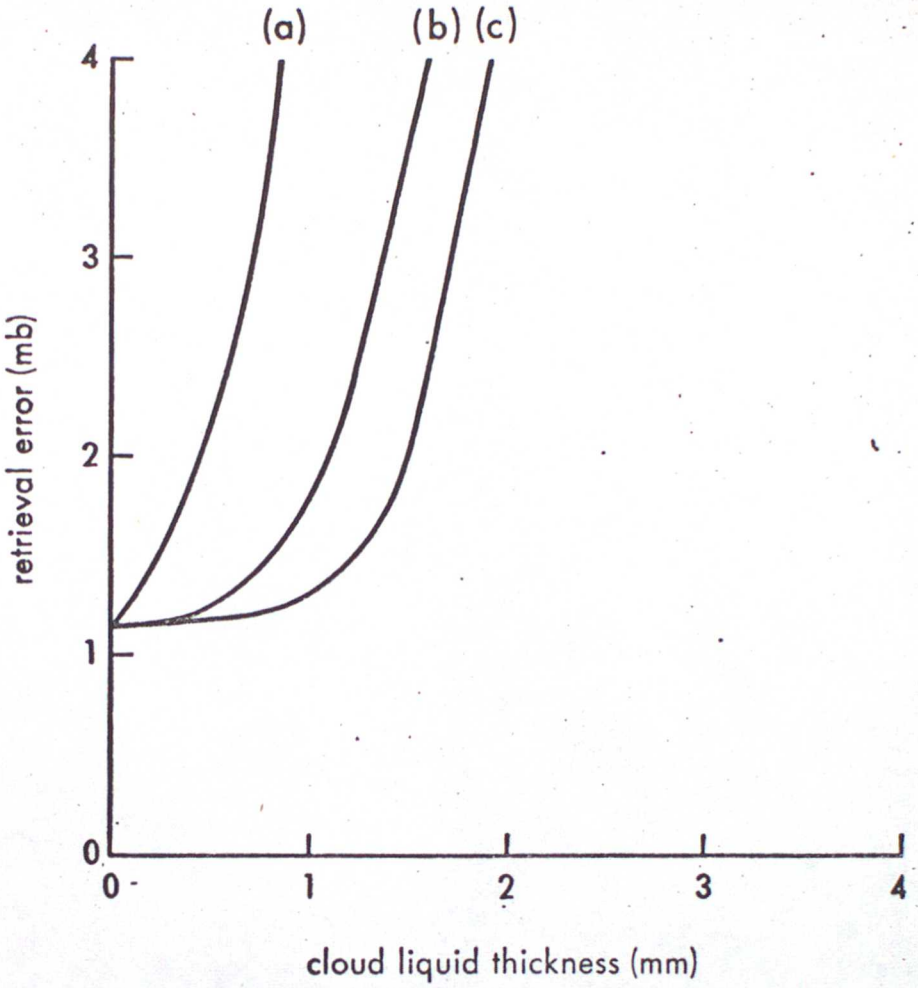

Figure 17.

As for Fig. 16 but with uniform rainfall rate of 4 mm/hr.

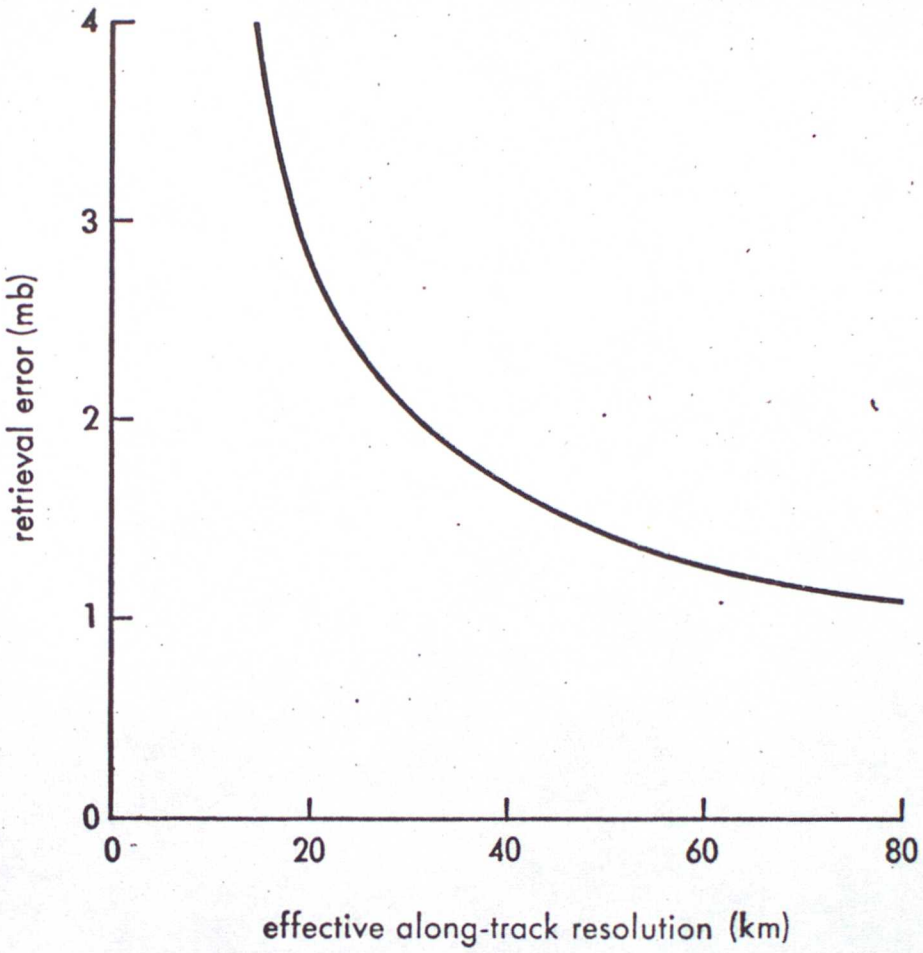

Figure 18.

Retrieval error due to loss of sea-statistics only against effective along-track resolution.

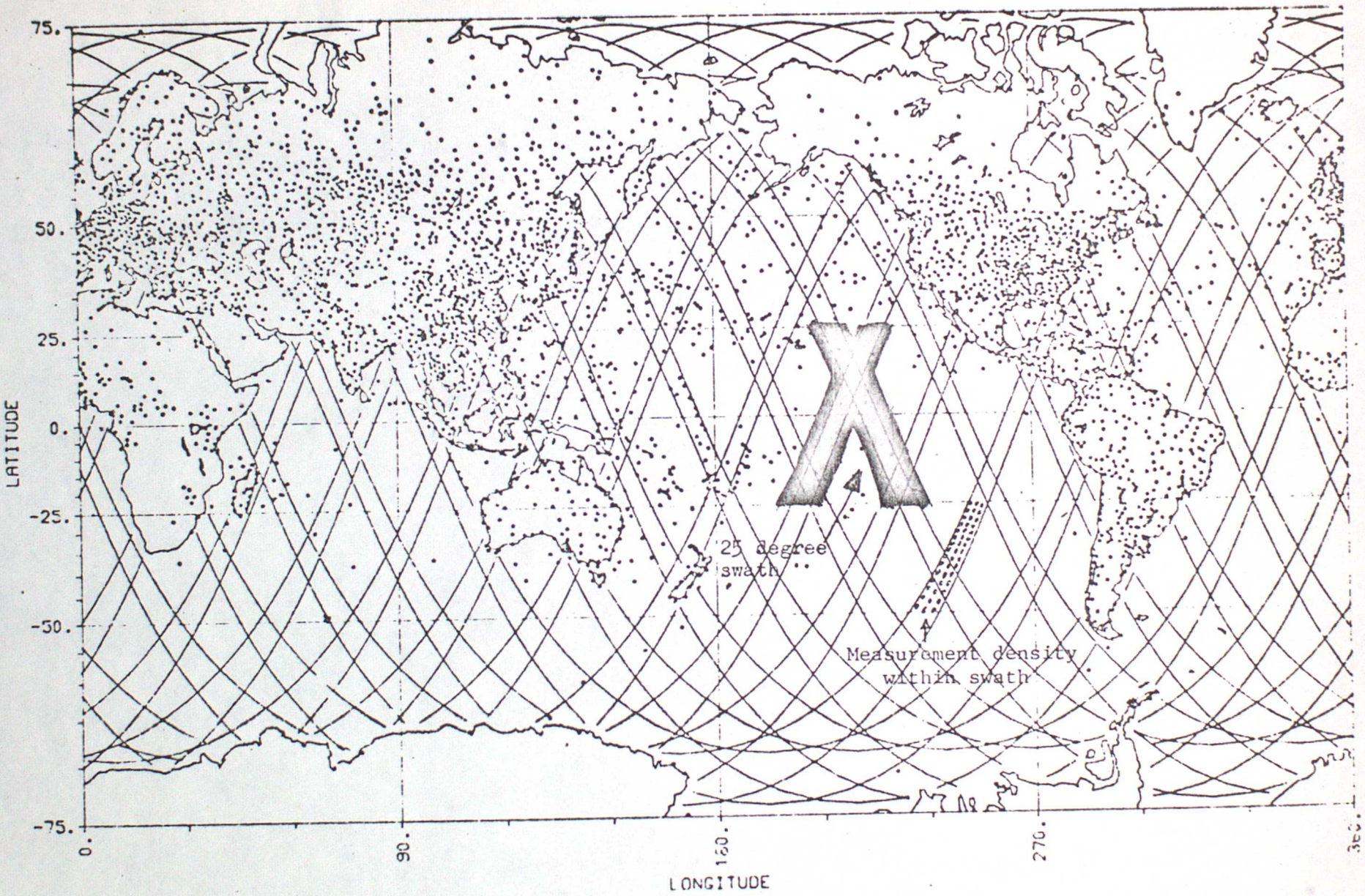

Figure 19 Potential daily coverage of surface pressure measurement with MPS in a SEASAT orbit compared with present coverage. From [1] . Dark region shows partial coverage with 25 degree off-nadir beam.

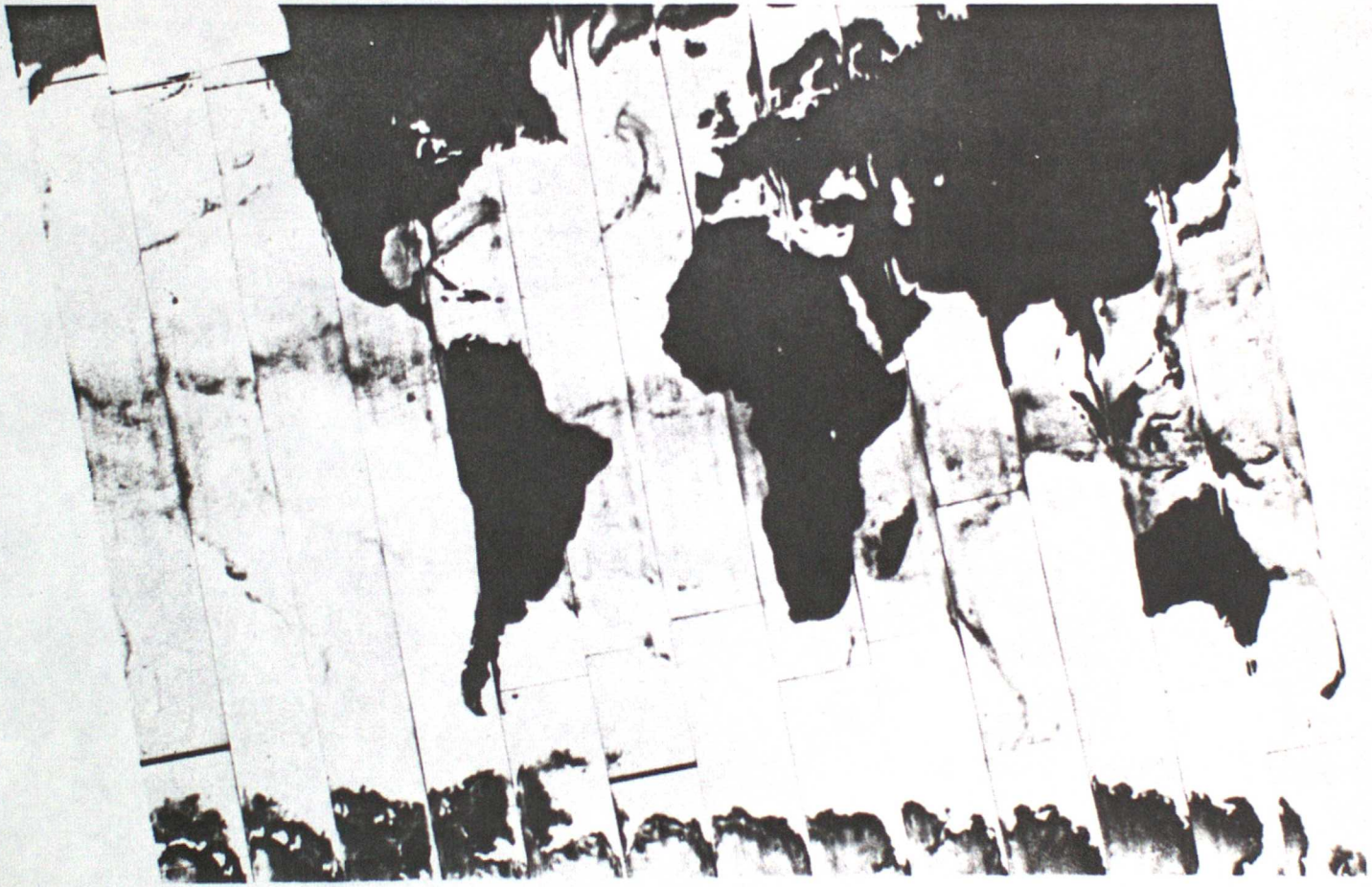

Figure 20 Photographically processed Nimbus 5 ESMR data from 11 January 1973, orbits 413-425. Brightness temperatures less than 190 K are white, those greater than 250 K are black, and those in between are represented by a linear gray scale. Rain, which appears dark over the ocean is evident in the tropics and in several weather fronts. (From The Nimbus 5 Data Catalog, Vol. 1)

From [21]

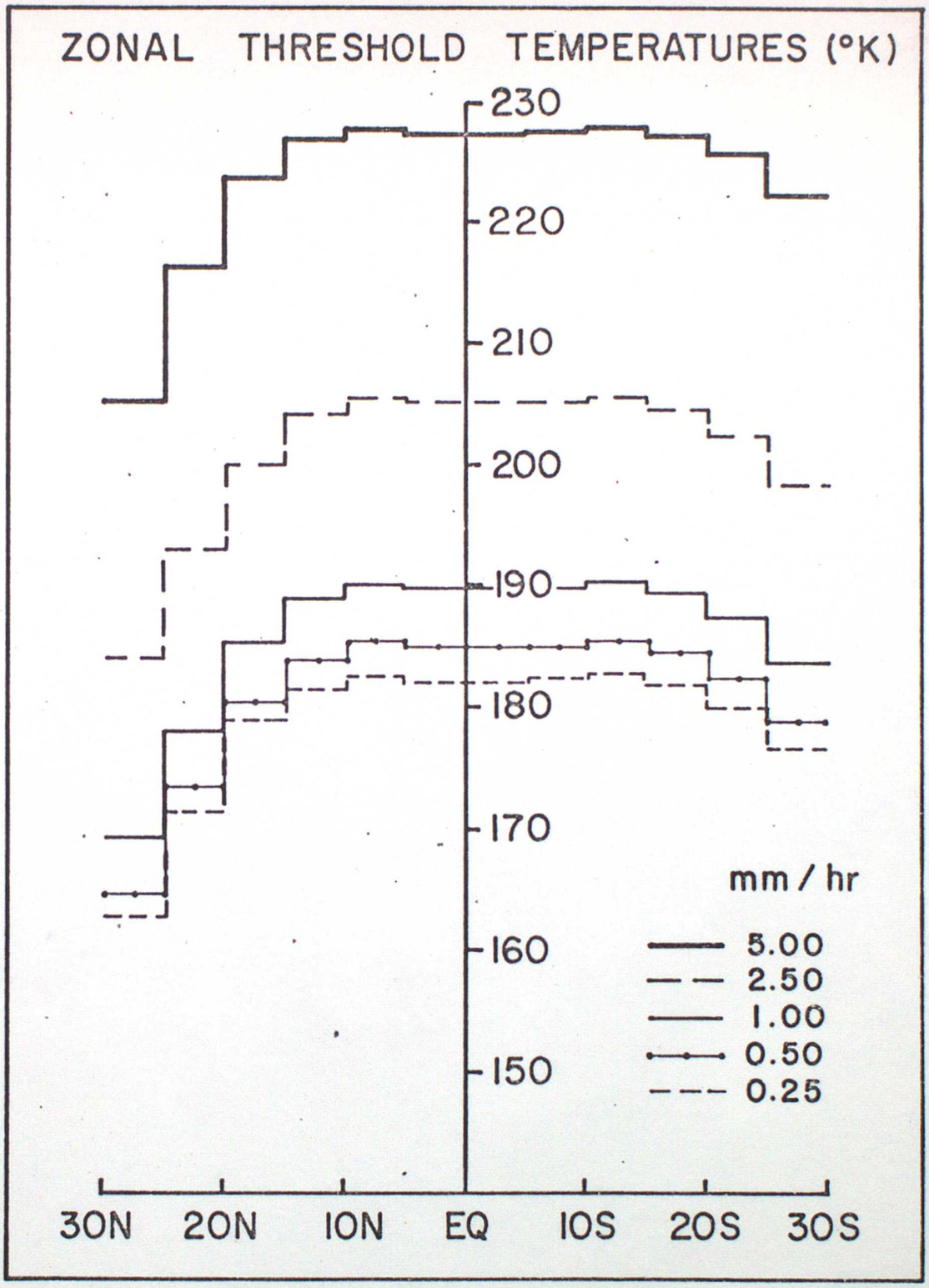

Figure 21. Zonal 1.55 cm threshold brightness temperatures for the detection of oceanic precipitation during the season December-January-February.

ESMR threshold =190K. From [21]

Figures 23-25

Numerical rainfall forecasts

.2mm/hr isopleths

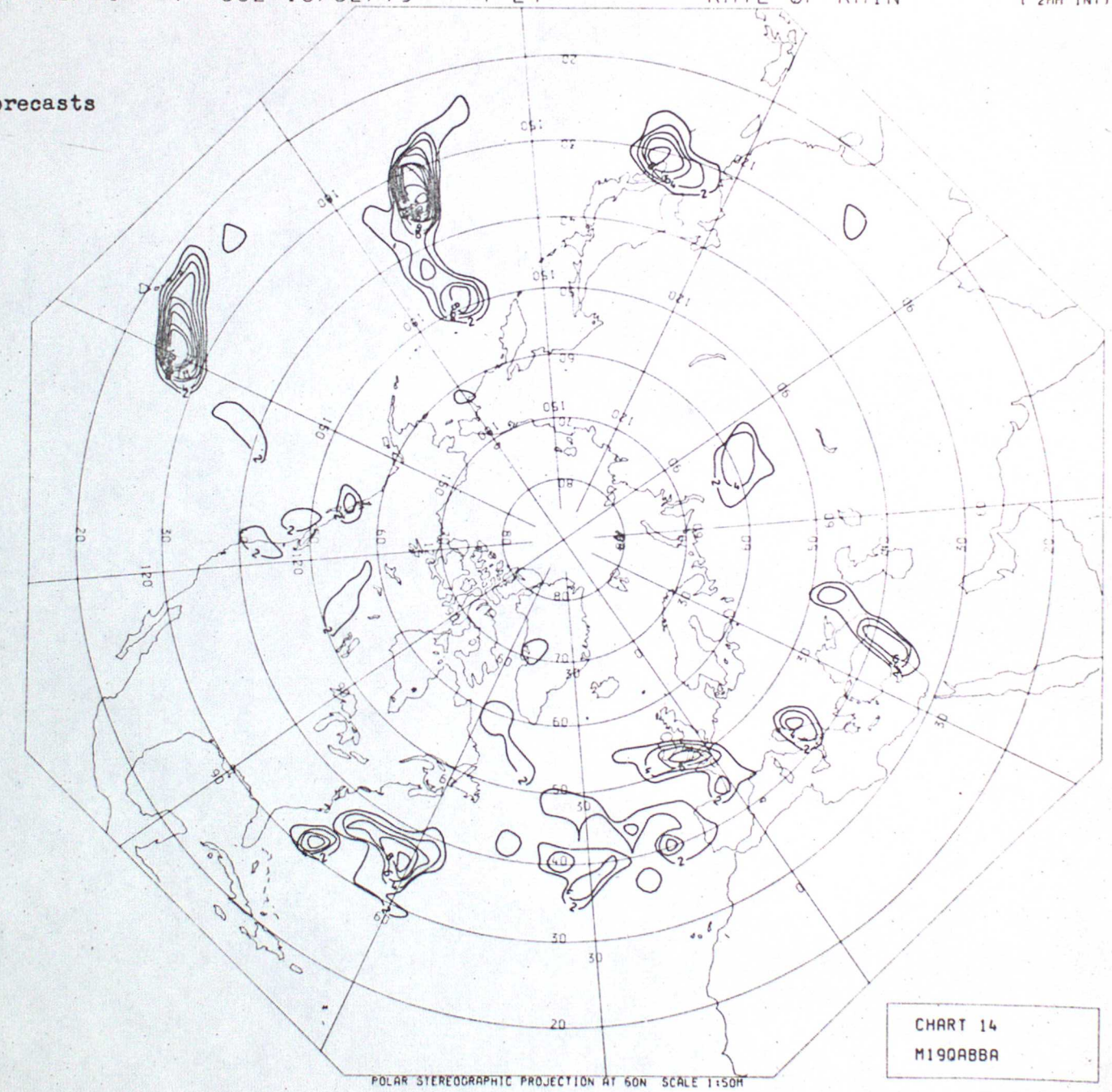

DT 12Z 12/02/79 VT 12Z 13/02/79 T+24 RATE OF RAIN (2MM INT)

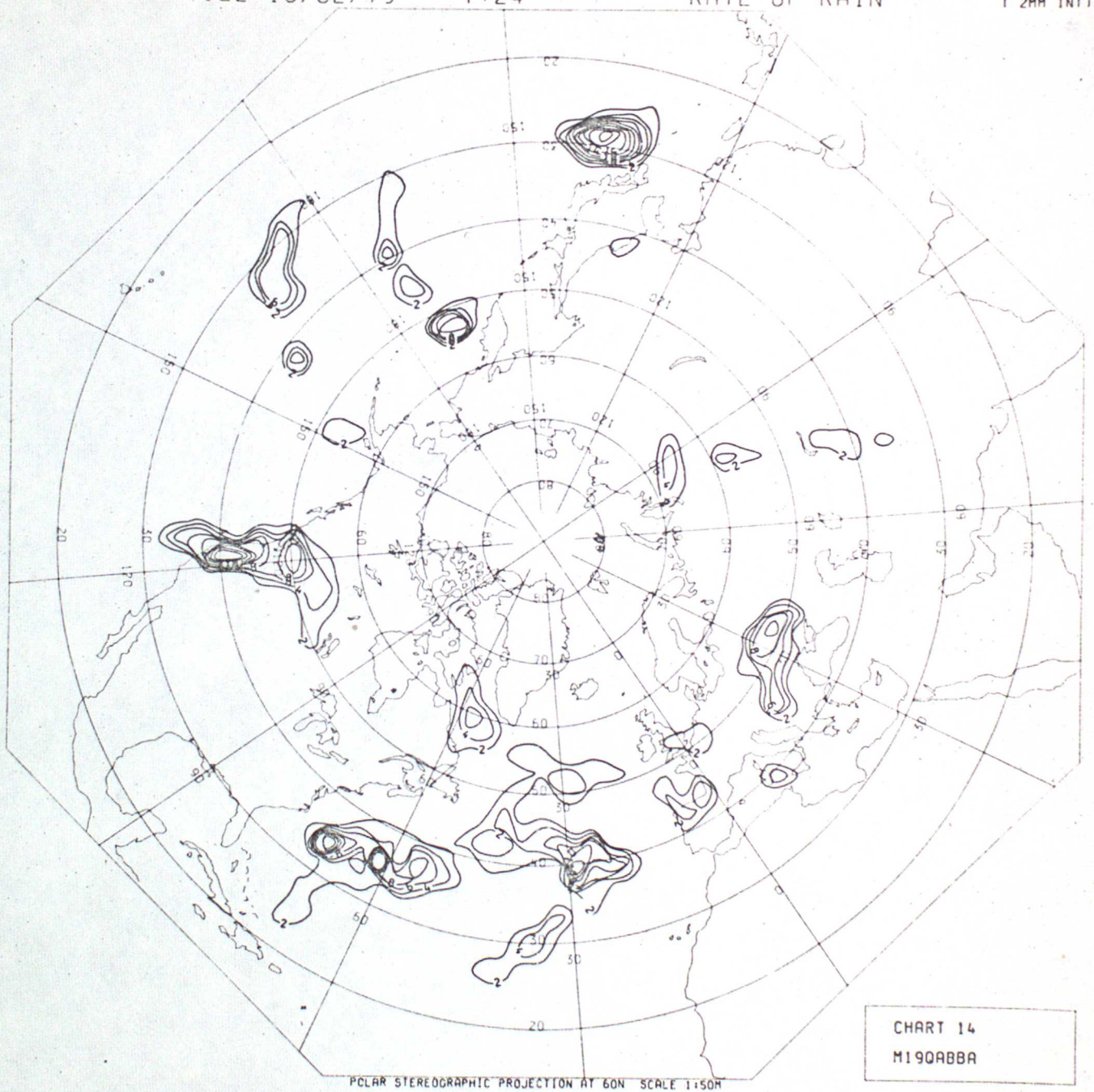

CHART 14
M19QABBA

DT 12Z 13/02/79 VT 12Z 14/02/79 T+24 RATE OF RAIN (2MM INT)

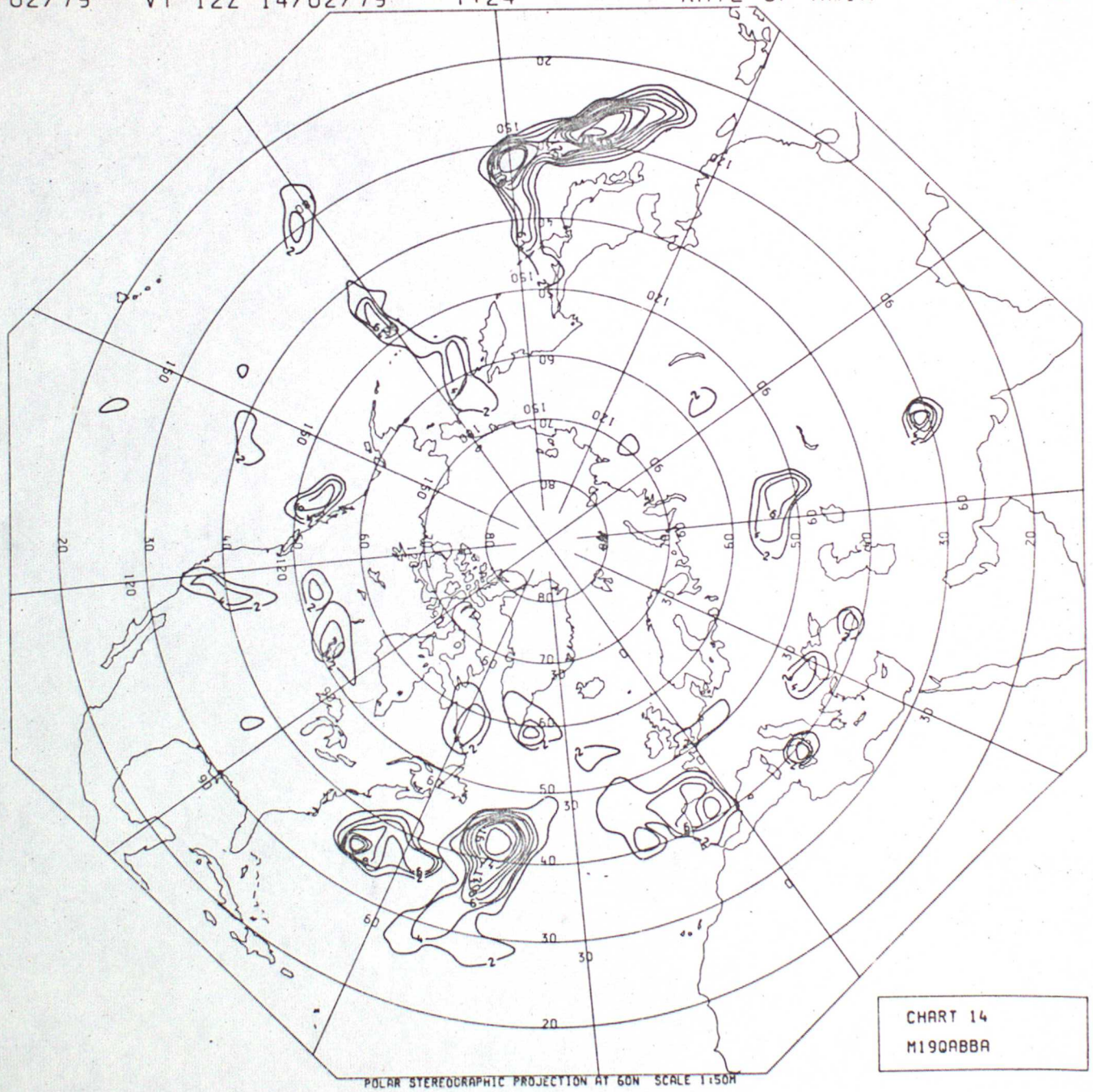

POLAR STEREOGRAPHIC PROJECTION AT 60N SCALE 1:50M

CHART 14
M19QABBA

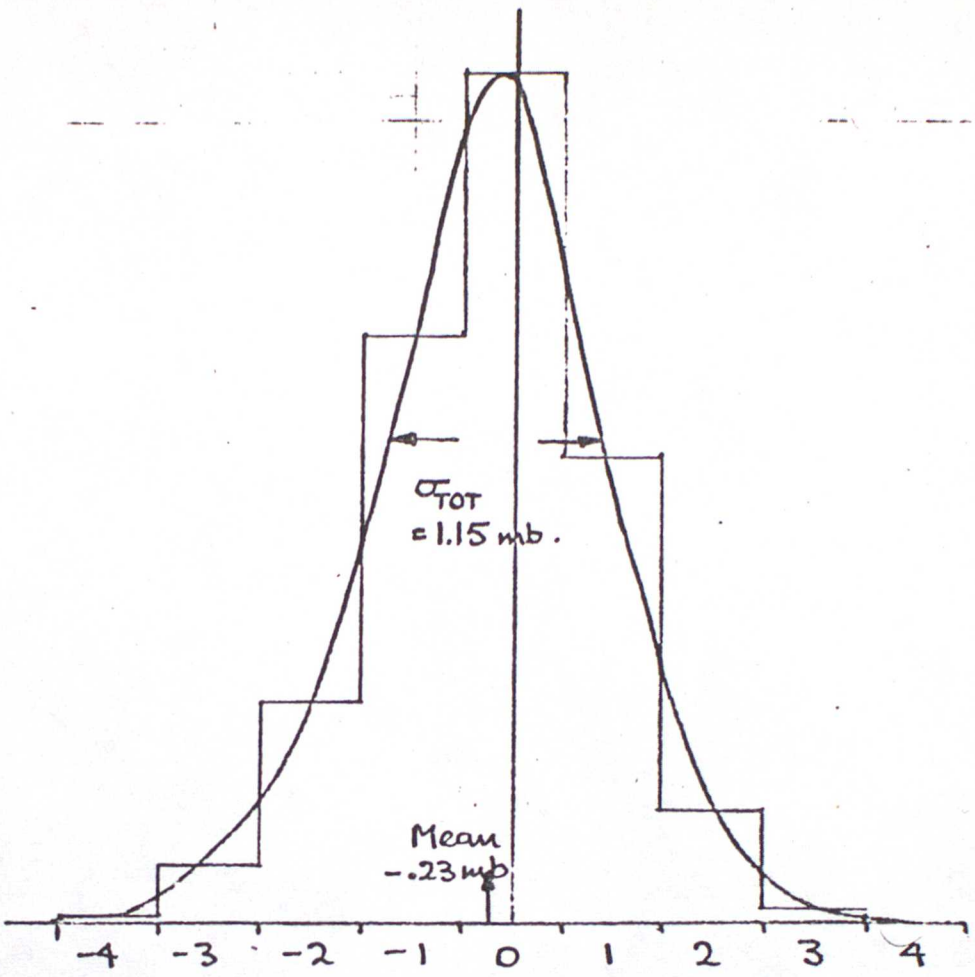

Error distribution		
	0 mb	32%
	1 mb	42%
	2 mb	13%
	3 mb	3%
	4 mb	1%
Data loss		9%.

Expected Distribution of Errors Fig 26

Taken from [23]